In Silico Analysis of Some Phytochemicals as Potential Anti-cancer Agents Targeting Cyclin Dependent Kinase-2, Human Topoisomerase IIa and Vascular Endothelial Growth Factor Receptor-2

Bishajit Sarkar[1*], Md. Asad Ullah[1], Syed Sajidul Islam[1]

[1]Department of Biotechnology and Genetic Engineering, Faculty of Biological Sciences, Jahangirnagar University, Savar, Dhaka, Bangladesh.

Corresponding author: Bishajit Sarkar[*]

Email of the corresponding author: sarkarbishajit@gmail.com

ORCID iD of the corresponding author: https://orcid.org/0000-0001-8439-6994

Abstract

Cancer is caused by a variety of pathways, involving various types of enzymes, among them three enzymes: cyclin dependent kinase-2 (CDK-2), human topoisomerase IIa and vascular endothelial growth factor receptor-2 (VEGFR-2) are three most common enzymes that involve in the cancer development. Although various drugs are available in the market, plant sources are known to contain a wide variety of agents that can be used to fight against cancer. In this experiment, total thirty compounds (ten compounds for each of the mentioned enzyme group) were analysed against the mentioned enzymes using various tools of in silico biology like molecular docking study, druglikeness property experiment, ADME/T test, PASS prediction and P450 site of metabolism prediction, pharmacophore modelling, DFT calculations and molecular dynamics simulation study to determine one best ligand (total three ligands for three enzymes) that have the capability to inhibit each of the mentioned enzymes. Form the experiment, epigallocatechin gallate was found to be the best ligand to inhibit CDK-2, daidzein showed best inhibitory activities towards human topoisomerase IIa and quercetin gave best performances against VEGFR-2 and they were also found to be quite safe and effective agents to treat cancer.

Keywords: molecular docking, quercetin, epigallocatechin gallate, daidzein, cancer.

1. Introduction

Cancer is defined as the uncontrolled proliferation and abnormal spread of the body's specific cells. According to WHO, 13% of world deaths accounted in 2005 is because of cancer. Moreover, projections have shown that cause-specific years of life lost (YLL) rate due to cancer would increase in 2005, 2015 and 2030. Millions of species of plants, animals, marine organisms and microorganisms act as attractive sources for new therapeutic candidate compounds. However, the development of novel agents from natural sources face many obstacles that are not usually met when one deals with synthetic compounds. Moreover, there may be difficulties with identification, isolation, assessing and obtaining the appropriate amounts of the active compound in the sample. (1, 2) The search for anti-cancer compounds from plant sources started in earnest in the 1950s with the discovery and development of the various natural compounds like vinca alkaloids, vinblastine, vincristine and cytotoxic podophyllotoxins. The successful clinical utilization of cancer chemotherapeutic agents from higher plants for about half a century has made the researchers more interested to conduct such types of explorations. In the recent years, new technologies have been developed by the scientists to enhance natural product drug discovery in an industrial manner. Indeed, several new anticancer agents of natural origin have been introduced to the market recently and there is a promising pipeline of natural products in cancer-related clinical trials from various types of organisms (3, 4, 5, 6). Future advances in the directed biosynthesis of small molecules will be driven by a mixture of technology and creativity. These advances will improve the ability of the scientists to control the shape and topology of various small molecules and thus allowing to create new anti-cancer compounds that interact specifically with biological targets. In the future, plants (300,000–500,000 such species) will continue to be a vital and valuable resource for anticancer drug discovery. More than 60 compounds from different plant sources are currently in the pipeline as potential anticancer agents (7, 8, 9, 10). There are many pathways that are involved in the cancer development. Strategy to develop anti-cancer drug usually involves blocking one or more components of specific pathway that is involved in the cancer development. In this experiment, thirty phytochemicals were analyzed against three enzymes (Cyclin Dependent Kinase-2 (CDK-2), Human Topoisomerase IIa and Vascular Endothelial Growth Factor Receptor-2 (VEGFR-2) of three different pathways involved in cancer development (**Table 01**, **Figure 01** and **Figure 02**).

Table 01. List of the plant derived anti-cancer agents that work via CDK-2, human topoisomerase IIa and VEGFR-2 pathways.

No	Name of the agents	References
01	Remangiflavonone B	(11)
02	Epigallocatechin gallate	(12, 13)
03	Indirubin	(14, 15)
04	Fisetin	(16, 17)
05	Apigenin	(16; 18)
06	Luteolin	(16; 19)
07	Kaempferol	(16; 20)
08	Chrysin	(16; 21)
09	Elenoside	(11)
10	Genistein	(16; 22)
11	Amentoflavone	(23)
12	Cryptolepine	(24, 25)
13	Neocryptolepine	(26, 27)
14	Bakuchicin	(28)
15	Lunacridine	(29)
16	Daidzein	(30)
17	Camptothecin	(31)
18	Salvicine	(32, 33)
19	Sauchinone	(34)
20	Nectandrin B	(34)
21	Ellagic acid	(35, 36)
22	Dioscin	(37, 38)
23	12-Deoxyphorbol 13-palmitate	(39)
24	Melatonin	(40)
25	5-hydroxy tryptophol	(40)
26	α-santalol	(41)
27	Plumbagin	(42)
28	Decursin	(43, 44)
29	Decursinol	(43, 45)
30	Quercetin	(46, 47)

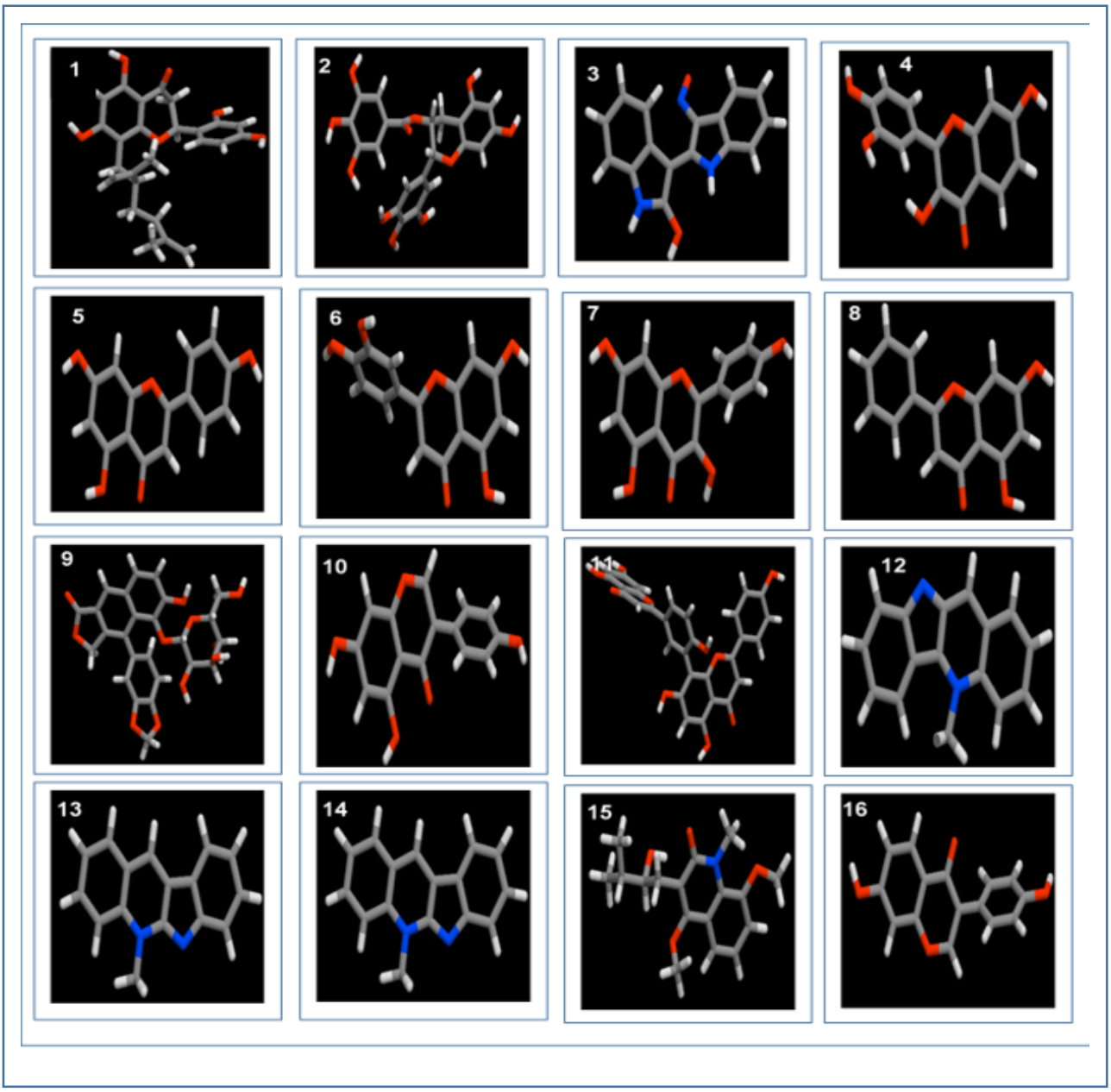
1
2
3
4
5
6
7
8
9
10
11
12
13
14
15
16

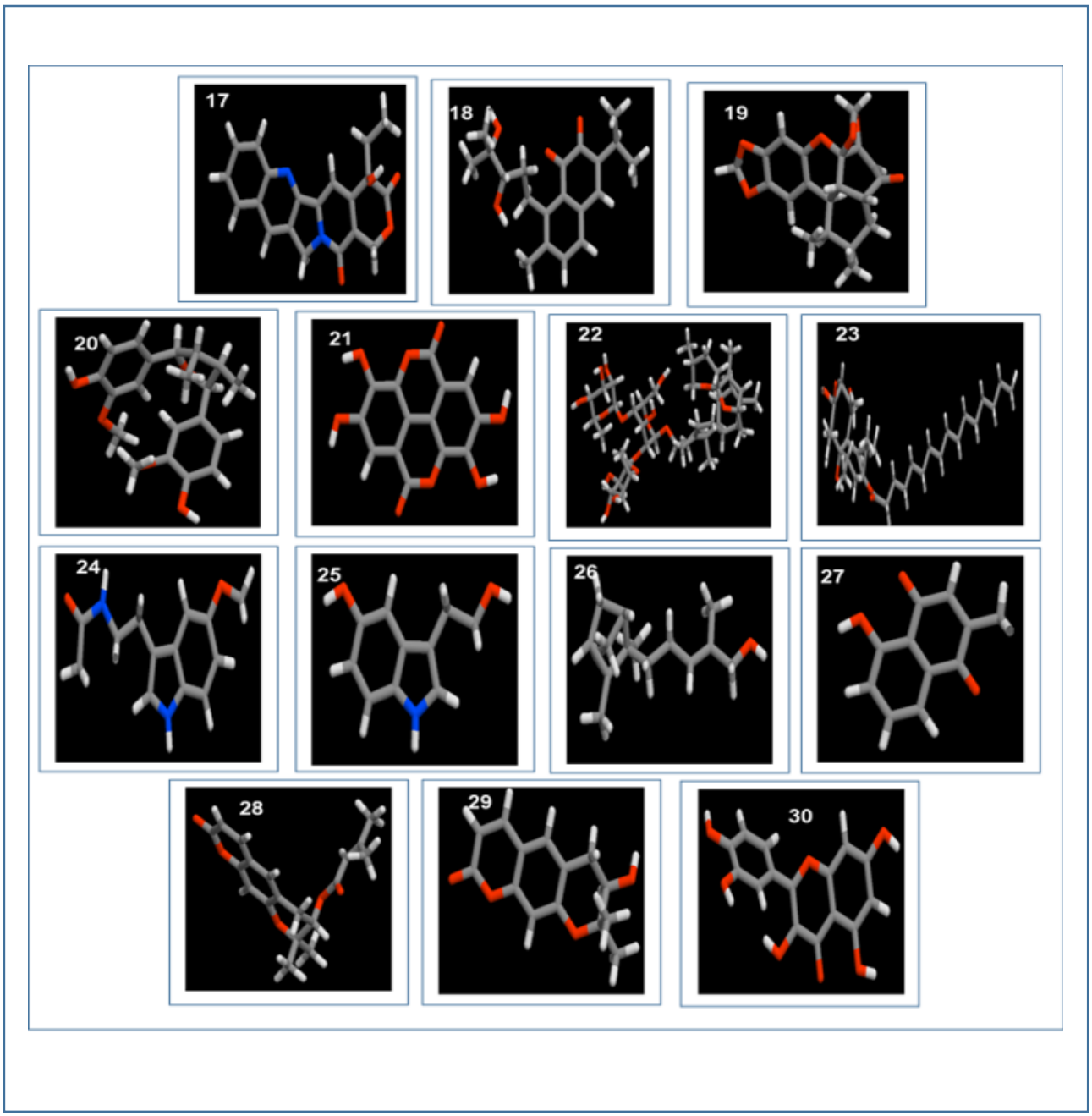

Figure 01. 3D structures of the 30 ligands used in the experiment. The 3D structures were generated by Galaxy 3D generator tool of online server Molinspiration Chemoinformatics (https://www.molinspiration.com/). Here, 1. Remangiflavanone B, 2. Epigallocatechin gallate, 3. Indirubin, 4. Fisetin, 5. Apigenin, 6. Luteolin, 7. Kaempferol, 8. Chrysin, 9. Elenoside, 10. Genistein, 11. Amentoflavone, 12. Cryptolepine, 13. Neocryptolepine, 14. Bakuchicin, 15. Lunacridine, 16. Daidzein, 17. Camptothecin, 18. Salvicine, 19. Sauchinone, 20. Nectandrin B, 21. Ellagic acid, 22. Dioscin, 23. 12-Deoxyphorbol 13-palmitate, 24. Melatonin, 25. 5-hydroxy tryptophol, 26. α-santalol, 27. Plumbagin, 28. Decursin, 29. Decursinol and 30. Quercetin.

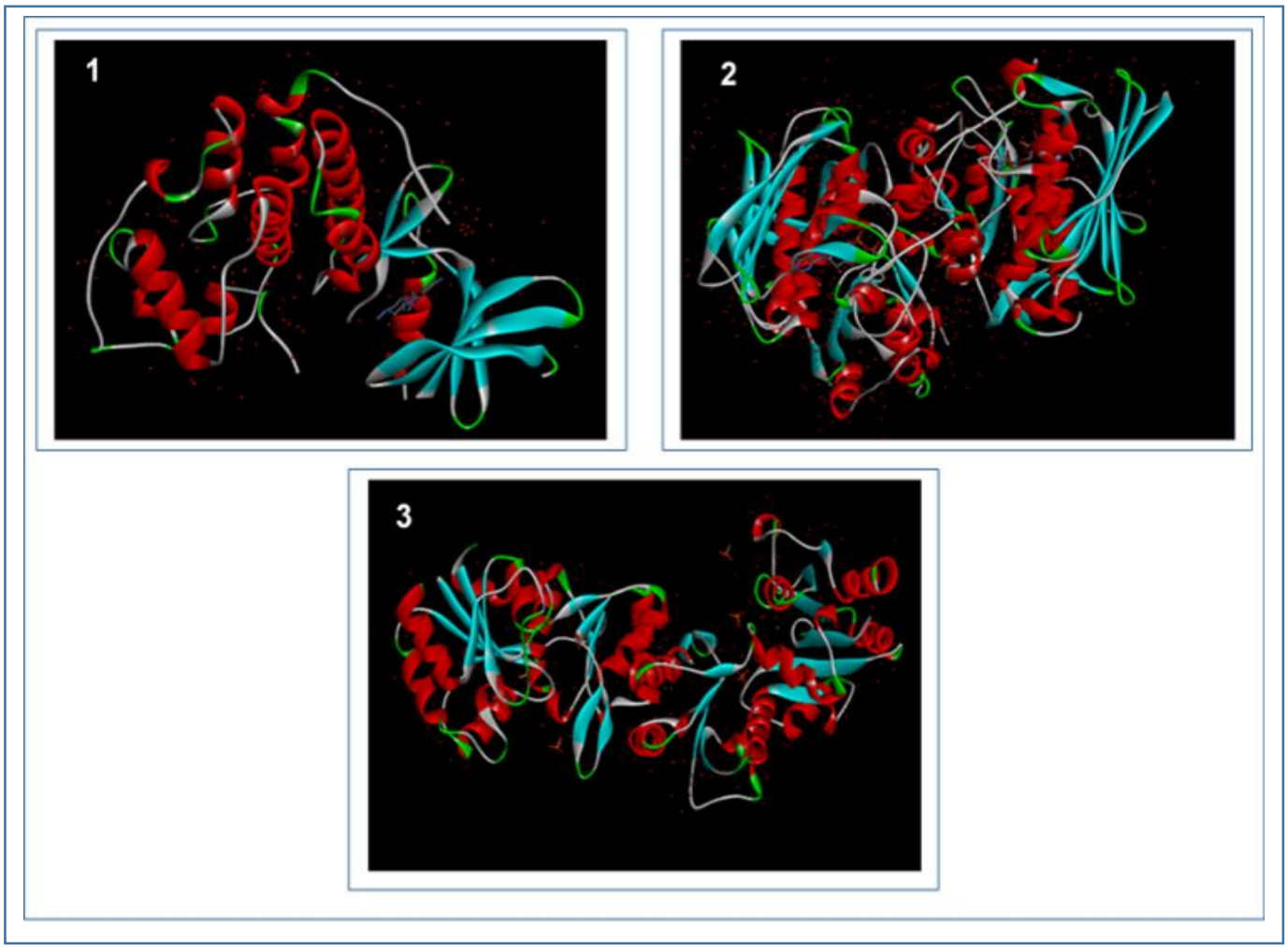

Figure 02. The 3D structures of the target proteins, 1. Cyclin dependent kinase-2 (PDB ID: 3EZV); 2. Human topoisomerase IIa (PDB (ID: 1ZXM); 3. Vascular endothelial growth factor receptor-2 (PDB ID: 2OH4). The 3D structures were visualized by Discovery Studio Visualizer.

1.1. 1.1. Role of Cyclin Dependent Kinase-2 (CDK-2) in cyclin/CDK Pathway and Its Involvement in Cancer

The cell cycle is regulated by different distinct pathways and cyclin/CDK pathway is one of the major cell cycle regulatory pathways. This pathway involves the cyclin-dependent kinases (CDKs), Retinoblastoma (Rb) tumor suppressor family and a family of transcription factors known as E2F. All these components of the pathway are essential for the passage of cells through the G1 to the S phase of the cell cycle. The CDK proteins are serine/threonine kinase that phosphorylate and thus inactivate the Rb protein. In the cell, the Rb protein forms complex with the transcription factor E2F. In the resting state of cell, Rb inhibits the activity of E2F protein forming a complex with it. The cyclin proteins can be of D type (cylcin D) and E type (cyclin E). Upon activation by the growth promoting signals or several mitogens, the cyclin D is found to form complex with CKD-4 and CKD-6. However, the cyclin E is found to be associated with CKD-2, when it is activated by active E2F. The cyclin D-CDK-4/6 and cyclin E-CDK-2 complexes phosphorylate and thereby inactivate the Rb protein. This inactivation causes the release of bound E2F transcription factor from the Rb protein. The released E2F later takes part in cell cycle progression. Moreover, E2F also promotes the activation of Cyclin E-CDK-2 complex, which in turn phosphorylates Rb protein and activate E2F transcription factor by feedback loop. Many inhibitors of the CDK proteins also takes part to regulate the cell cycle properly. The inhibitors repress the CDK proteins when there is no need for the cells to divide (48, 49, 50, 51, 52, 53, 54). The inhibitors are proteins from inhibitors of CDK-4 (INK4) and cyclin-dependent kinase inhibitor (CKI) families. CDK-4/6 is inhibited by p15/16 inhibitors and CDK-2 is inhibited by p21/p27 inhibitors. However, any type of mutation in the CDK genes causing hyperactivity or any type of mutation in the inhibitory genes, may lead to the uncontrolled proliferation of the cells, which can lead to different forms of cancers (55). For this reason, the targeting and inhibition of CDK-2 is a potential strategy for anticancer drug development (56) (**Figure 03**). In the experiment, ten selected ligand molecules: remangiflavanone B, genistein, indirubin, elenoside, epigallocatechin gallate, fisetin, apigenin, luteolin, kaempferol and chrysin, were used to dock against the CDK-2 enzyme. Alvocidib, a known inhibitor of CDK-2 that is currently in pre-clinical trials, was used as positive control to make comparison of binding affinity with the selected ligands (11).

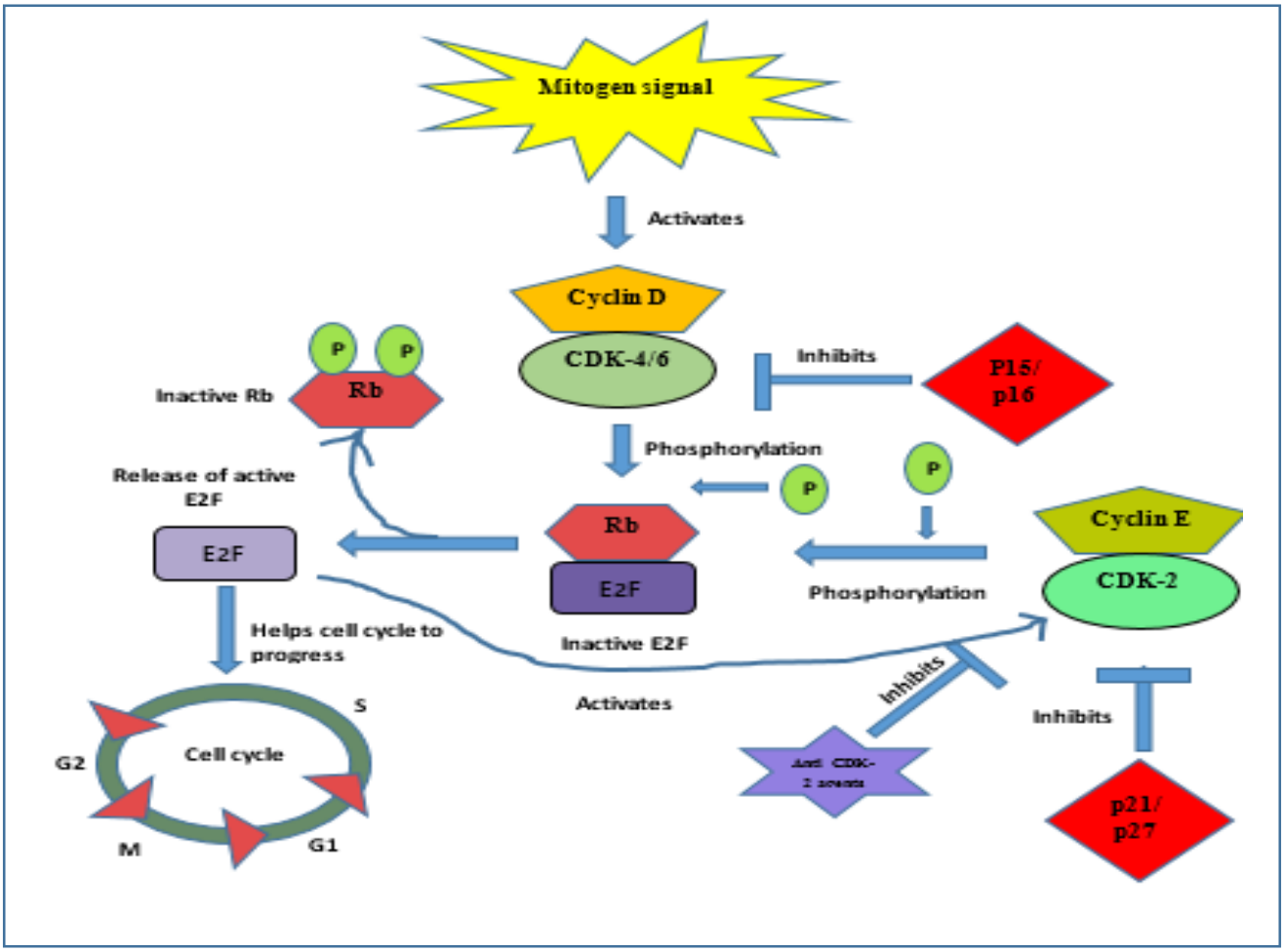

Figure 03. The cyclin/CDK signalling pathway. Upon activated by mitogen signal, the cyclin D-CDK-4/6 complex is activated and cause the inactivation of Rb by phosphorylation and thus release the active E2F, which takes part in cell cycle progression. However, E2F activates cyclin E-CDK-2 complex, which phosphorylates the Rb protein and activates the E2F in a feedback loop. P15/p16 inhibitors repress cyclin D-CDK-4/6 complex and p21/p27 inhibit cyclin E-CDK-2. Anti-CDK-2 agents inhibit the CDK-2 protein, thus can help in cancer treatment.

1.2. The DNA Topoisomerase IIa Pathway and Its Involvement in Cancer

Due to the supercoiled structure of the DNA molecules, it is necessary to unwind the double stranded DNA before replication, transcription, recombination, segregation and other processes. DNA topoisomerases are the enzymes that functions in the unwinding of DNA double helix structure. They cut, shuffle and relegate the DNA double helix structure. The human genome encodes six topoisomerases that are grouped into three types: type IA, type IB and type IIA. DNA topoisomerase IIa is one the necessary topoisomerases that function in various cellular functions. However, DNA topoisomerase II is a genotoxic enzyme which can lead to cancer development. When DNA topoisomerase II cuts the double stranded DNA, it may remain covalently attached to the broken end of the DNA. This reaction intermediate is known as the cleavage complex. The cleavage complexes are temporary structures and are essential for many cellular functions. However, if the amount of the cleavage complex in the cell falls too much, the cells are not able to divide into daughter cells due to mitotic failure, which results in the death of the cells. Moreover, if the amount of the cleavage complex increases too much, the temporary cleavage complex structures can become permanent double stranded breaks in the DNA. These double stranded breaks are caused by the faulty DNA tracking system which then initiate the faulty recombination and repair pathways of DNA that leads to abnormal DNA translocations and mutagenesis as well as DNA abnormality, leading to cancer (**Figure 04**). For this reason, DNA topoisomerase IIa is considered as the potential target for anti-cancer drug dvelopment (57, 58, 59, 60). In this experiment, ten selected ligand molecules: amentoflavone, cryptolepine, neocryptolepine, bakuchicin, lunacridine, daidzein, camptothecin, salvicine, sauchinone and nectandrin B, were used to dock against human topoisomerase IIa. Daunorubicin is a FDA approved drug to treat cancer that targets human topoisomerase IIa (61). It is a known DNA topoisomerase IIa inhibitor that was used as the control to evaluate the binding affinity of the selected ligands with topoisomerase IIa.

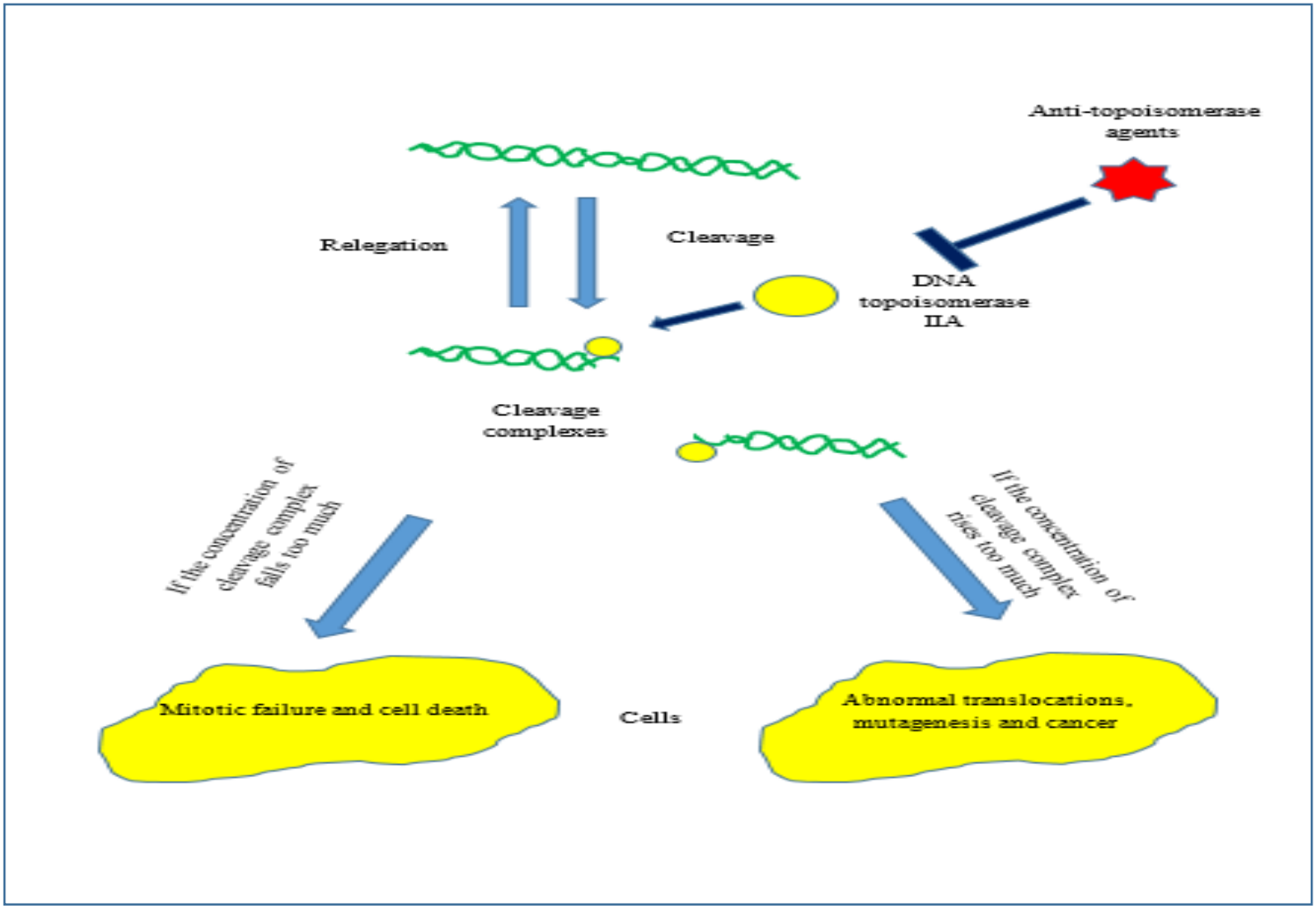

Figure 04. The DNA topoisomerase IIA pathway in cancer development. Upon the cleavage of the target DNA, the topoisomerase can remain bound to the cleaved ends of the DNA fragments and form cleavage complexes. If the concentration of cleavage complexes falls too much, then this may lead to cell death due to the mitotic failure. Moreover, if the concentration rises too much, abnormal translocations and mutagenesis may occur, which lead to cancer development. Anti-topoisomerase agents aid in cancer treatment by inhibiting the activity of DNA topoisomerase IIA.

1.3. The Role of Vascular Endothelial Growth Factor Receptor- 2 (VEGFR-2) in Angiogenesis Pathway and Its Involvement in Cancer

Angiogenesis is the process of generating new capillary blood vessels (62). It plays important functions in organ development and differentiation during embryogenesis as well as wound healing and reproductive functions. However, angiogenesis is also responsible for a number of disorders including tumor formation, cancers, rheumatoid arthritis etc. Vascular Endothelial Growth Factor (VEGF) plays key role in angiogenesis process (63). VEGF protein has many isoforms and all of the isoforms mediate their effects by specific receptors known as VEGF receptors (VEGFRs) (64). VEGFRs are receptor tyrosine kinases (RTKs) and there are three main isoforms: VEGFR-1, VEGFR-2, VEGFR-3. However, the expression of VEGF proteins are found to be dramatically increased in various types of human cancers like lung, thyroid, breast, ovary, kidney, uterine cancers etc. (63). Since VEGF mediates its effects by binding to specific receptors, inhibitions of the actions of the receptors is thought to be a therapeutic target for cancer treatment. The VEGFR-2 is mainly associated with the angiogenesis in various tumors, for this reason, inhibiting VEGFR-2 can prevent tumor growth and cancer development (65). Several pathways involve in the angiogenesis during cancer development. All of the pathways are mediated by the interaction of VEGF protein(s) with VEGFR (in most cases VEGFR-2). When VEGF protein binds with VEGFR-2, the VEGFR-2 becomes activated which then activates phosphatidylinositol 3-kinase (PI3K). PI3K further activates phosphoinositide 3 kinase (PIP3), which in turn activates the Akt/PKB (protein kinase B) signaling pathway. This pathway contributes to endothelial cell survival by activating proteins, like BAD (Bcl-2 associated death promoter) and caspase proteins, that have functions in cell survival. Moreover, the Akt/PKB signaling pathway can activate the endothelial nitric-oxide synthase (eNOS), which is responsible for vascular permeability. Both the endothelial cell survival and vascular permeability mechanisms contribute to the angiogenesis process **(Figure 05)**. The binding of VEGF to VEGFR-2 can sometimes activate MAP kinase (mitogen activated protein kinase) pathway which is responsible for the proliferation of endothelial cells. In this pathway, activated VEGFR-2 activates phospholipase c-γ (PLC-γ). The PLC-γ then activates the protein kinase C (PKC). PKC further activates the proteins of MAP kinase pathway: RAF1, MEK, ERK, sequentially. This MAP kinase pathway causes the endothelial cell proliferation, which also contributes to the angiogenesis process **(Figure 05)** (66, 67, 68).

Since VEGFR-2 is involved in angiogenesis process in cancer development, inhibition of VEGFR-2 is considered as therapeutic approach to treat cancer. In this experiment, 10 selected ligands, ellagic acid, dioscin, 12-Deoxyphorbol 13-palmitate, melatonin, 5-hydroxy tryptophol, α-santalol, plumbagin, decursin, decursinol and quercetin, were used to dock against the VEGFR-2. Lenvatinib is a FDA approved drug that is used to treat cancer by targeting VEGFR-2 (69). Lenvatinib, a known inhibitor of VEGFR-2, was used as positive control for the comparison of binding affinities of the ligands with VEGFR-2 in this experiment.

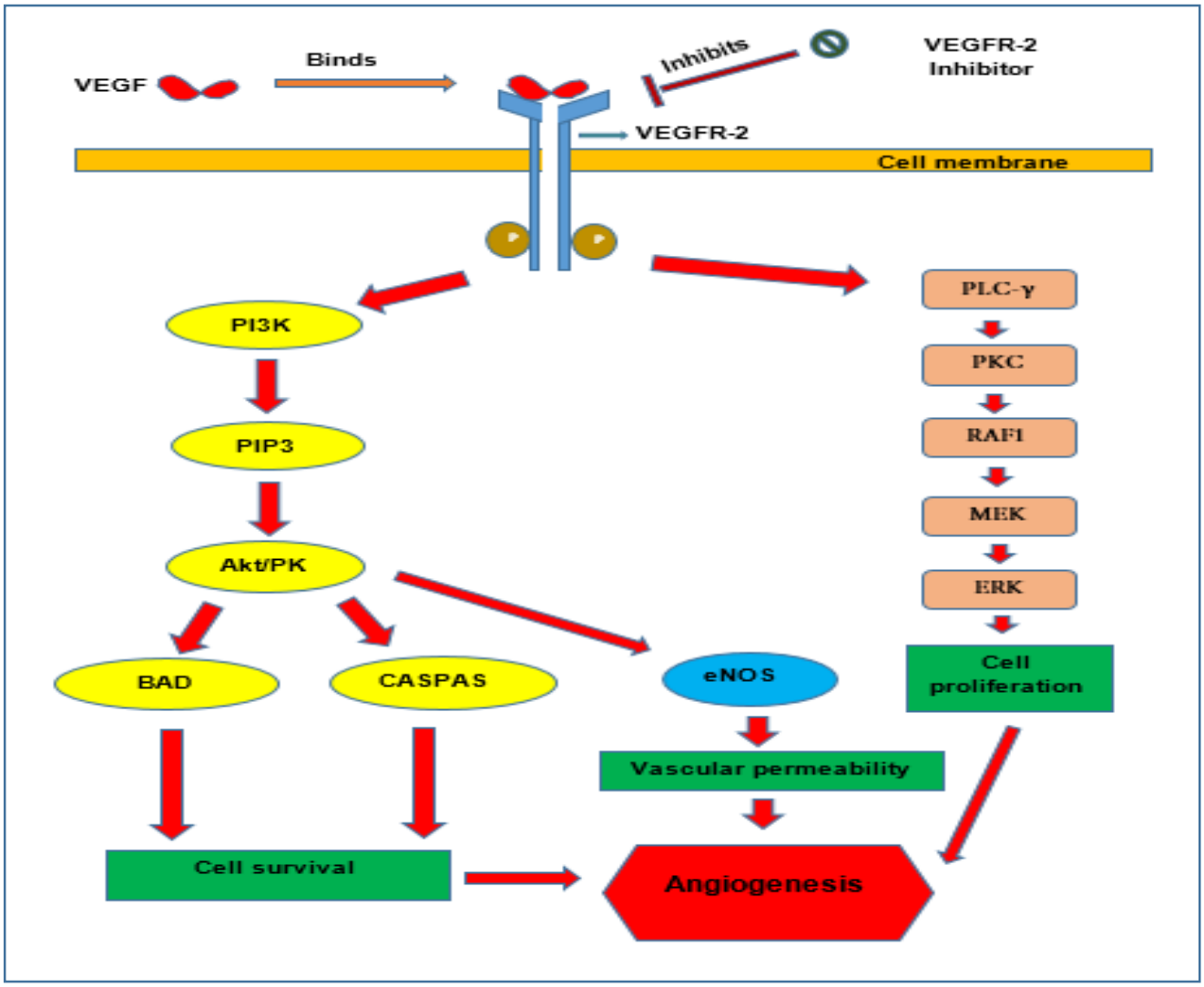

Figure 05. The angiogenesis pathway. The VEGF protein binds with VEGFR-2 and activates the receptor. The VEGFR-2 activates PI3K. PI3K further activates PIP3, which activates the Akt/PKB signaling pathway. This pathway contributes to endothelial cell survival by activating BAD and caspase proteins. Moreover, the Akt/PKB signaling pathway can activate eNOS, which is responsible for vascular permeability. Both the endothelial cell survival and vascular permeability mechanisms contribute to the angiogenesis process. The binding of VEGF to VEGFR-2 can sometimes activate MAP kinase pathway which is responsible for the proliferation of endothelial cells. The activated VEGFR-2 activates PLC-γ. The PLC-γ further activates PKC. PKC further activates RAF1, MEK, ERK, sequentially. This MAP kinase pathway causes the endothelial cell proliferation, which also contributes to the angiogenesis process. VEGFR-2 inhibitors inhibits VEGFR-2, thus aid in cancer treatment.

2. Materials and methods

In this experiment, total 30 ligand molecules (10 ligands for inhibiting each of the three receptors), that have potential anti-cancer effects, were first selected from extensive literature reviewing. After that, glide standard precision (SP) ligand docking were carried out for all the 30 ligands. Based on the lowest or best docking score, three ligands from each of the enzyme group were selected. Next, the free binding energy (ΔG_{Bind}) scores of the selected ligand molecules were calculated and they were then subjected to induced fit docking (IFD). Upon evaluation of the ΔG_{Bind} values, IFD scores and XP G_{score} one best ligand molecule was selected from each of the enzyme category. Positive controls were used only to compare the binding affinities but they were not utilized in the later experiments to determine the physiochemical and physiological properties of the selected best ligands. The ligand preparation, grid generation and glide docking, 2D representations of the best pose interactions between the three best ligands and their respective receptors were obtained using Maestro-Schrödinger Suite 2018-4. The 3D representations of the best pose interactions between the ligands and their respective receptors were visualized using Discovery Studio Visualizer (70, 71). The 2D structures of ligands were downloaded from PubChem in SDF format (www.pubchem.ncbi.nlm.nih.gov) and the receptors were downloaded from protein data bank (www.rcsb.org).

2.1. Protein Preparation and Ramachandran plot generation

Three dimensional structures of Cyclin-dependent kinase-2 (3EZV), Human topoisomerase II (1ZXM) and Vascular Endothelial Growth Factor Receptor-2 (2OH4) were downloaded (sequentially) in PDB format from protein data bank (www.rcsb.org). The proteins were then prepared and refined using the Protein Preparation Wizard in Maestro Schrödinger Suite 2018-4 (72). Bond orders were assigned and hydrogens were added to heavy atoms as well as all the waters were deleted and the side chains were adjusted using Prime (73). Finally, the structure was optimized and then minimized using force field OPLS_2005. Minimization was done setting the maximum heavy atom RMSD (root-mean-square-deviation) to 30 Å and any remaining water less than 3 H- bonds to non-water was again deleted during the minimization step. After successful minimization, the proteins were used to generate Ramachandran plots for each of the protein by Maestro Schrödinger Suite 2018-4, keeping all the parameters as default.

2.2. Ligand Preparation

Three dimensional structures of 30 selected ligand molecules as well as controls were downloaded (sequentially) from PubChem database (www.pubchem.ncbi.nlm.nih.gov). These structures were then prepared using the LigPrep function of Maestro Schrödinger Suite **(**74**)**. Minimized 3D structures of ligands were generated using Epik2.2 and within pH 7.0 +/- 2.0 (75). Minimization was again carried out using OPLS_2005 force field which generated 32 possible stereoisomers.

2.3. Receptor Grid Generation

Grid usually confines the active site to shortened specific area of the receptor protein for the ligand to dock specifically. In Glide, a grid was generated using default Van der Waals radius scaling factor 1.0 and charge cutoff 0.25 which was then subjected to OPLS_2005 force field. A cubic box

was generated around the active site (reference ligand active site). Then the grid box volume was adjusted to 15×15×15 for docking test.

2.4. Glide Standard Precision (SP) Ligand Docking, Prime MM-GBSA Calculation and Induced Fit Docking

SP adaptable glide docking was carried out using Glide in Maestro Schrödinger Suite (76). The Van der Waals radius scaling factor and charge cutoff were set to 0.80 and 0.15 respectively for all the ligand molecules. Final score was assigned according to the pose of docked ligand within the active site of the receptor. The ligand with lowest glide docking score was considered as the best ligand. After successful docking, the 2D representations of the best pose interactions between the ligands and their respective receptors were generated using Maestro-Schrödinger Suite.

After SP ligand docking three ligands were selected from each enzyme category (total 9) which were then again subjected to MM-GBSA (Molecular mechanics – generalized born and surface area) rescoring using the Prime module of Maestro Schrödinger suite for further evaluation. This technique utilizes the docked complex and uses an implicit solvent which then assigns more accurate scoring function and improves the overall free binding affinity score upon the reprocessing of the complex. It combines OPLS molecular mechanics energies (E_{MM}), surface generalized born solvation model for polar solvation (G_{SGB}), and a nonpolar salvation term (G_{NP}) for total free energy (ΔG_{bind}) calculation. The total free energy of binding was calculated by the following equation:

$$\mathbf{\Delta G_{bind} = G_{complex} - (G_{protein} - G_{ligand}), \text{ where, } G = E_{MM} + G_{SGB} + G_{NP}}$$

To carry out the IFD of the best 9 selected ligand molecules, again OPLS_2005 force field was applied after generating grid around the co-crystallized ligand of the receptor and this time the best five ligands were docked rigidly. Receptor and Ligand Van Der Waals screening was set at 0.70 and 0.50 respectively, residues within 2 Å were refined to generate 2 best possible posses with extra precision. Best performing ligand was from each enzyme category was selected according to the $\mathbf{\Delta G_{bind}}$, IFD score and XP_{Gscore}.

The 3D representations of the best pose interactions between the ligands and their respective receptors were obtained using Discovery Studio Visualizer (71).

2.5. Ligand Based Drug Likeness Property and ADME/Toxicity Prediction

The drug likeness properties of the selected ligand molecules were analyzed using SWISSADME server (http://www.swissadme.ch/) as well as the OSIRIS Property Explorer (https://www.organic-chemistry.org/prog/peo/) (77). The ADME/T for each of the ligand molecules was carried out using online based servers, admetSAR (http://lmmd.ecust.edu.cn/admetsar2/) and ADMETlab (http://admet.scbdd.com/) to predict their various pharmacokinetic and pharmacodynamic properties. Both admetSAR and ADMETlab servers are comprehensive tools to determine the absorption, distribution, metabolism, excretion and toxicity of various drug and chemical compounds (78, 79). The absorption, distribution and metabolism properties were determined by admetSAR server and excretion and toxicity properties were determined by ADMETlab server. The numeric and categorical values of the results given by ADMETlab server were changed into

qualitative values according to the explanation and interpretation described in the ADMETlab server (http://admet.scbdd.com/home/interpretation/) for the convenience of interpretation.

2.6. PASS (Prediction of Activity Spectra for Substances) and P450 Site of Metabolism (SOM) prediction

The PASS (Prediction of Activity Spectra for Substances) prediction of the three best selected ligands were conducted by using PASS-Way2Drug server (http://www.pharmaexpert.ru/passonline/) by using canonical SMILES from PubChem server (https://pubchem.ncbi.nlm.nih.gov/) (80). To carry out PASS prediction, P_a (probability "to be active") was kept greater than 70%, since the $P_a > 70\%$ threshold gives highly reliable prediction (81). In the PASS prediction study, both the possible biological activities and the possible adverse effects of the selected ligands were predicted. The P450 Site of Metabolism (SOM) of the three best selected ligand molecules were determined by online tool, RS-WebPredictor 1.0 (http://reccr.chem.rpi.edu/Software/RS-WebPredictor/) (82). The LD50 and Toxicity class was predicted using ProTox-II server (http://tox.charite.de/protox_II/) (83). The canonical SMILES of epicatechin was taken from PubChem server (https://pubchem.ncbi.nlm.nih.gov/) and the SMILES was used to predict the LD50 and toxicity class.

2.7. Pharmacophore Modelling

The pharmacophore modelling of the three best ligands were carried out using the Phase pharmacophore perception engine of Maestro-Schrödinger Suite (84). The pharmacophore modelling was done manually. To carry out the process, the radii sizes were kept as the Van der Waals radii of receptor atoms, radii scaling factor was kept at 0.50, receptor atoms whose surfaces are within 2.00 Å of the ligand surface were ignored and the volume shell thickness was limited to 5.00 Å.

2.8. Solubility Prediction

The solubility testing of the best three ligands were performed using the QikProp wizard of Maestro-Schrödinger Suite (85). In solubility prediction, the solubility of the selected ligands were determined in various interfaces like hexadecane/gas interface, octanol/gas interface, octanol/water interface etc.

2.9. DFT Calculations

Minimized ligand structures obtained from LigPrep were used for DFT calculation using the Jaguar panel of Maestro Schrödinger Suite using Becke's three-parameter exchange potential and Lee-Yang-Parr correlation functional (B3LYP) theory with 6-31G* basis set (86, 87, 88). Quantum chemical properties such as surface properties (MO, density, potential) and Multipole moments were calculated along with HOMO (Highest Occupied Molecular Orbital) and LUMO (Lowest Unoccupied Molecular Orbital) energy. Then the global frontier orbital was analyzed and hardness (**η**) and softness (**S**) of selected molecules were calculated using the following equation as per Parr and Pearson interpretation and Koopmans theorem (89, 90). The DFT calculation was done for the 3 best ligand molecules.

$$\eta = (HOMO\varepsilon - LUMO\varepsilon)/2, \quad S = 1/\eta$$

2.10. Molecular Dynamics Simulation

The molecular dynamics simulation study of the best three ligands, epigallocatechin gallate, daidzein and quercetin and their respective receptors, were performed by the online server iMODS (http://imods.chaconlab.org/). The server is a fast, user-friendly and effective molecular dynamics simulation tool that can be used efficiently to investigate the structural dynamics of the protein complexes. The server provides the values of deformability, B-factor (mobility profiles), eigenvalues, variance, co-varience map and elastic network. For a complex or protein, the deformability depends on the ability to deform at each of its amino acid residues. The eigenvalue has relation with the energy that is required to deform the given structure and the lower the eigenvalue, the easier the deformability of the complex. Moreover, the eigenvalue also represents the motion stiffness of the protein complex. The server is a fast and easy server for determining and measuring the protein flexibility (91, 92, 93, 94, 95). For analysing the molecular dynamics simulation of the three complexes, the docked PDB files were uploaded to the iMODS server and the results were displayed keeping all the parameters as default.

3. Results

3.1. Ramachandran Plot and Molecular Docking Analysis

After preparing the proteins, the Ramachandran plot for each of the receptor proteins was generated. In the plot window, glycine is presented as triangles, proline is presented as squares and all other residues are presented as circles. Moreover, the orange regions are designated as "favored" regions, the yellow regions are designated as "allowed" regions and the white regions are designated as "disallowed" regions (96). CDK-2 protein generated Ramachandran plot with only a few amino acids in the “allowed” region and almost all of the amino acids in the “favored” region. It had no amino acids in the “disallowed region”. Human topoisomerase II generated Ramachandran plot with 15 amino acids in the “disallowed region”. It also had majority of the amino acids in the “favored” region. VEGFR-2 generated Ramachandran plot with only 4 amino acids in the “disallowed” region and most of the amino acids in the “favored” region (**Figure 06).**

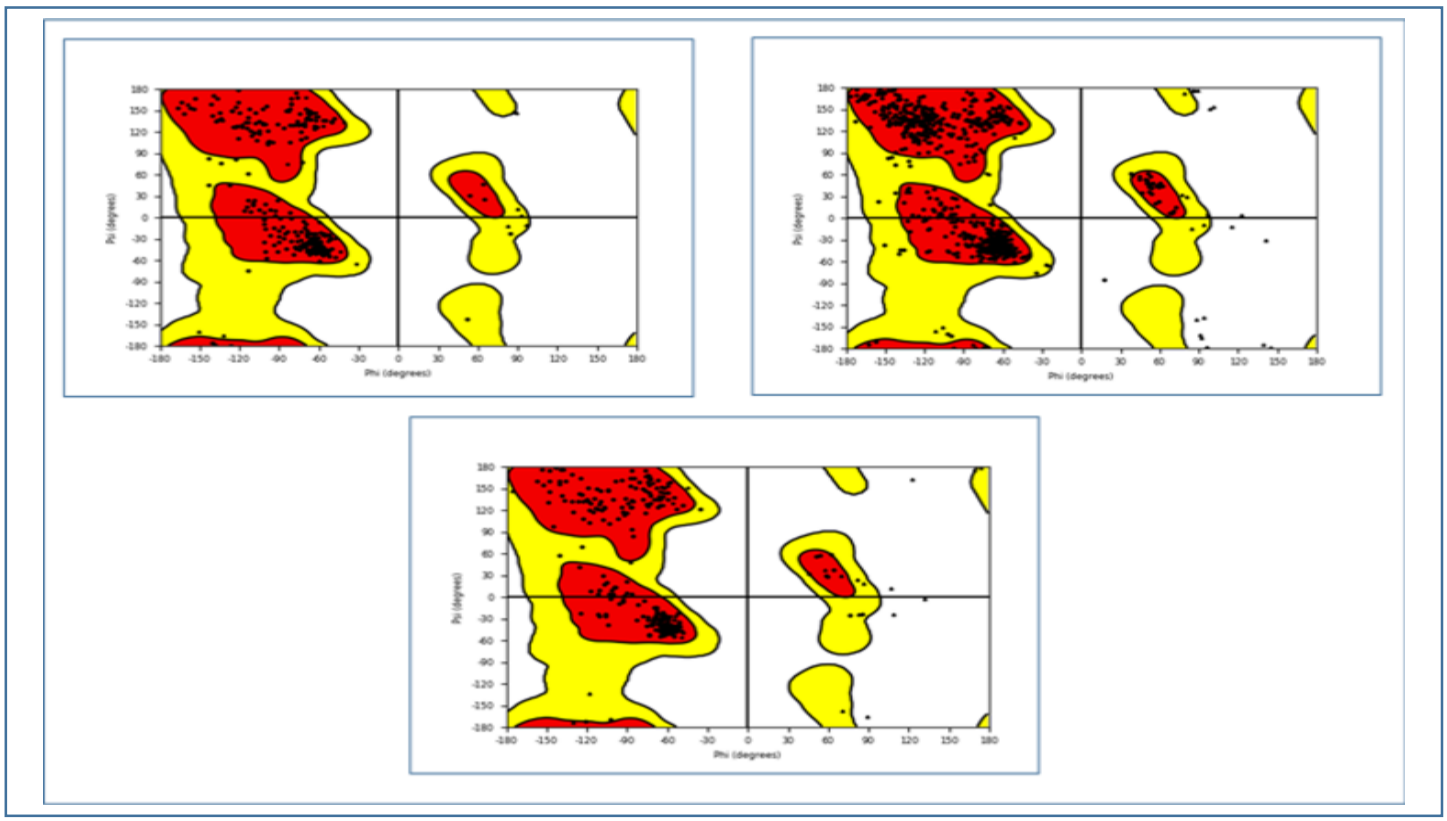

Figure 06. Ramachandran plot analysis of 1. CDK-2, 2. Human topoisomerase II, 3. VEGFR-2. Glycine and proline are represented as triangles and squares and all other amino acids are represented as spheres. CDK-2 had no amino acids in the "disallowed region". Human topoisomerase II had 15 amino acids: Lys 276 (residue A), Gly 322 (residue A & B), Gly 69 (residue A & B), Gly 52 (residue B), Gly 323 (residue A & B), Gly 283 (residue B), Gly 406 (residue B), Gly 266 (residue A & B), Gly 122 (residue A & B) and VEGFR-2 had 4 amino acid: Gly 891 (residue A), Gly 1061 (residue A), Gly 1120 (residue A), Gly 844 (residue A), in the "disallowed region.

All the selected ligand molecules were docked successfully with their respective receptor proteins. The ligand molecules that had the lowest binding energy were considered the best ligand molecules in inhibiting their respective receptors since lower binding energy (docking score) corresponds to higher binding affinity (97, 98, 99).

10 agents, remangiflavanone B, epigallocatechin gallate, indirubin, fisetin, apigenin, luteolin, kaempferol, chrysin, elenoside and genistein were against CDK-2. Based on the lower docking score or binding energy, 3 ligands: remangiflavanone B (-7.341 Kcal/mol), epigallocatechin gallate (-7.123 Kcal/mol) and indirubin (-8.410 Kcal/mol) were selected for MM-GBSA and IFD studies. The control alvocidib showed docking score of -4.144 Kcal/mol. (**Table 02**).

Amentoflavone, cryptolepine, neocryptolepine, bakuchicin, lunacridine, daidzein, camptothecin, salvicine, sauchinone and nectandrin B were the 10 selected ligand molecules that were used to dock against human topoisomerase II. Based on the lower binding energy, daidzein (-7.855 Kcal/mol), camptothecin (-7.630 Kcal/mol) and salvicine (-6.969 Kcal/mol), were selected for MM-GBSA and IFD studies. The control daunorubicin showed docking score of -2.469 Kcal/mol (**Table 02**).

Another receptor protein, VEGFR-2 was used to perform docking with another 10 ligand molecules and based on the lower docking score, quercetin (10.441 Kcal/mol), decursinol (-8.960 Kcal/mol) and plumbagin (-7.848 Kcal/mol) were selected as the three molecules for carrying out the MM-GBSA and IFD studies. The control lenvatinib showed docking score of -10.745 Kcal/mol (**Table 02**).

All the ligand molecules with their respective docking score and glide energy are listed in **Table 02**.

Table 02. The results of molecular docking study between the selected 30 ligands and their receptors. The docking was carried out using Maestro-Schrödinger Suite 2018-4.

No	Name of receptor (PDB ID)	Name of ligand (PubChem CID)	Docking score/ binding energy (Kcal/mol)	Glide energy (Kcal/mol)
Control-1	Cyclin-dependent kinase-2 (PDB ID: 3EZV)	Alvocidib (PubChem CID: 5287969)	-4.144	-42.707
01	Cyclin-dependent kinase-2 (PDB ID: 3EZV)	Remangiflavanone B (PubChem CID: 10741001)	-7.341	-48.430
02	Cyclin-dependent kinase-2 (PDB ID: 3EZV)	Epigallocatechin gallate (PubChem CID: 65064)	-7.123	-60.544
03	Cyclin-dependent kinase-2 (PDB ID: 3EZV)	Indirubin (PubChem CID: 10177)	-8.410	-33.776
04	Cyclin-dependent kinase-2 (PDB ID: 3EZV)	Fisetin (PubChem CID: 5281614)	-6.017	-42.105
05	Cyclin-dependent kinase-2 (PDB ID: 3EZV)	Apigenin (PubChem CID: 5280443)	-5.836	-36.499
06	Cyclin-dependent kinase-2 (PDB ID: 3EZV)	Luteolin (PubChem CID: 5280445)	-4.954	-38.551
07	Cyclin-dependent kinase-2 (PDB ID: 3EZV)	Kaempferol (PubChem CID: 5280863)	-4.046	-39.418
08	Cyclin-dependent kinase-2 (PDB ID: 3EZV)	Chrysin (PubChem CID: 5281607)	-5.893	-34.446
09	Cyclin-dependent kinase-2 (PDB ID: 3EZV)	Elenoside (PubChem CID: 10458570)	-7.036	-56.435
10	Cyclin-dependent kinase-2 (PDB ID: 3EZV)	Genistein (PubChem CID: 5280961)	-5.591	-37.710
Control-2	Human topoisomerase II (PDB ID: 1ZXM)	Daunorubicin (PubChem CID: 30323)	-2.469	-34.191
11	Human topoisomerase II (PDB ID: 1ZXM)	Amentoflavone (PubChem CID: 5281600)	-3.524	-32.638

12	Human topoisomerase II (PDB ID: 1ZXM)	Cryptolepine (PubChem CID: 82143)	-5.802	-40.963
13	Human topoisomerase II (PDB ID: 1ZXM)	Neocryptolepine (PubChem CID: 390526)	-5.277	-39.058
14	Human topoisomerase II (PDB ID: 1ZXM)	Bakuchicin (PubChem CID: 3083848)	-5.638	-37.756
15	Human topoisomerase II (PDB ID: 1ZXM)	Lunacridine (PubChem CID: 442920)	-5.413	-42.872
16	Human topoisomerase II (PDB ID: 1ZXM)	Daidzein (PubChem CID: 5281708)	-7.855	-42.546
17	Human topoisomerase II (PDB ID: 1ZXM)	Camptothecin (PubChem CID: 24360)	-7.630	-48.500
18	Human topoisomerase II (PDB ID: 1ZXM)	Salvicine (PubChem CID: 10359290)	-6.969	-42.072
19	Human topoisomerase II (PDB ID: 1ZXM)	Sauchinone (PubChem CID: 11725801)	-6.266	-42.390
20	Human topoisomerase II (PDB ID: 1ZXM)	Nectandrin B (PubChem CID: 156517)	-6.173	-43.608
Control-3	Human topoisomerase II (PDB ID: 1ZXM)	Lenvatinib (PubChem CID: 9823820)	-10.745	-61.045
21	Vascular Endothelial Growth Factor Receptor-2 (PDB ID: 2OH4)	Ellagic acid (PubChem CID: 5281855)	-5.039	-34.384
22	Vascular Endothelial Growth Factor Receptor-2 (PDB ID: 2OH4)	Dioscin (PubChem CID: 119245)	-3.524	-33.341
23	Vascular Endothelial Growth Factor Receptor-2 (PDB ID: 2OH4)	12-Deoxyphorbol 13-palmitate (PubChem CID: 322885)	-6.471	-51.617
24	Vascular Endothelial Growth Factor Receptor-2 (PDB ID: 2OH4)	Melatonin (PubChem CID: 896)	-6.996	-36.512
25	Vascular Endothelial Growth Factor	5-hydroxy tryptophol (PubChem CID: 9061)	-7.179	-28.520

	Receptor-2 (PDB ID: 2OH4)			
26	Vascular Endothelial Growth Factor Receptor-2 (PDB ID: 2OH4)	α-santalol (PubChem CID: 11085337)	-6.494	-23.456
27	Vascular Endothelial Growth Factor Receptor-2 (PDB ID: 2OH4)	Plumbagin (PubChem CID: 10205)	-7.848	-37.639
28	Vascular Endothelial Growth Factor Receptor-2 (PDB ID: 2OH4)	Decursin (PubChem CID: 442126)	-6.307	-38.690
29	Vascular Endothelial Growth Factor Receptor-2 (PDB ID: 2OH4)	Decursinol (PubChem CID: 442127)	-8.960	-34.149
30	Vascular Endothelial Growth Factor Receptor-2 (PDB ID: 2OH4)	Quercetin (PubChem CID: 5280343)	-10.441	-47.972

In the next step, the MM-GBSA and IFD studies were performed using the 9 selected ligands (three from each of the receptor group) as well as the controls to determine one best possible ligand from each of the 3 receptor groups. One best possible ligand, from each of the receptor category, was selected based on the ΔG_{Bind} score, XP G_{Score} and IFD score. In the MM-GBSA study, the most negative ΔG_{Bind} score (the lowest score) is considered as the best ΔG_{Bind} score (100). IFD study is done to understand the accurate binding mode and to ensure the accuracy of active site geometry. XP G_{Score} and IFD score are generated in the IFD experiment, which is an empirical scoring function that estimates the ligand binding free energy. The lowest values of IFD score and XP G_{Score} are considered as the best values and are always appreciable (101, 102, 103, 104). Among the three ligands that inhibited CDK-2, epigallocatechin gallate was selected as the best ligand in this step, although epigallocatechin gallate showed the second best ΔG_{Bind} score of -56.420 Kcal/mol, it had the lowest XP G_{Score} and IFD value. The 2D and 3D representations of the epigallocatechin gallate also confirms that it interacted with many amino acids in the binding vicinity of the receptor (**Figure 07** and **Figure 08**). On the other hand, among the 3 ligands selected based on the docking scores from the initial 10 ligands from the human topoisomerase IIa receptor category, daidzein gave the best result in the MM-GBSA and generated quite good results in IFD studies. For this reason, it was considered as the best possible ligand among the three selected ligands that inhibited human topoisomerase II. The 2D, 3D representations as well as interaction of different amino acids with daidzein are illustrated in **Figure 07** and **Figure 08**. Quercetin, decursinol and plumbagin were selected as the three best ligands, among the ten ligands that were used to dock against VEGFR-2. Since quercetin showed the best results in both the MM-GBSA and IFD studies, it was selected as the best ligand among the three selected ligand molecules (**Figure 07** and **Figure 08**). The controls: alvocidib, daunorubicin and lenvatinib showed ΔG_{Bind} scores of -72.500 Kcal/mol, -36.326 Kccal/mol and -103.240 Kcal/mol, respectively and XP G_{Score} values of -8.305 Kcal/mol, -6.455 Kcal/mol and -13.121 Kcal/mol, respectively. All the nine ligands and the the controls with their ΔG_{Bind} scores, XP G_{Score} values and IFD scores as well as number of hydrogen bonds and interacting amino acids are listed in **Table 03**. The three best selected ligands, with their interacting amino acids, distances of the bonds, their interaction category and types of interaction are listed in **Table 04**.

Now, these 3 best ligands (one from each of the receptor category) were used to carry out further analysis to determine their safety and efficacy.

Table 03. The results of MM-GBSA and IFD studies between the three best ligands and their respective receptors, along with their interaction with different types of amino acids.

Name of receptor	**Name of ligand**	**MM-GBSA (ΔG_{Bind} Score Kcal/mol)**	**XP G_{Score} (Kcal/mol)**	**IFD score (Kcal/mol)**	**No of hydrogen bonds**	**Interacting amino acids**
Cyclin dependent kinase-2	Remangiflavanone B	-74.370	-8.531	-593.230	06	Leu 55, Val 64, Leu 134, Ala 144, Phe 80, Phe 146, Ala 31, Asp 135, Lys 33, Val 18
	Epigallocatechin gallate	-56. 420	-8.616	-594.990	07	Lys 89, Leu 289, His 84, Glu 08, Ile 10, Leu 134, Gln 131
	Indirubin	-49.960	-6.636	-587.810	02	Leu 134, Asp 86, Gln 131, Ile 10, Val 18, Ala 31
Control- 1	Alvocidib	-72.500	-8.305	-591.005	03	Asp 145, Ala 144, Leu 134, Asp 86, Gln 131, Ile 10, Val 18, Ala 31
Human topoisomerase II	Daidzein	-55.980	-8.152	-1730.510	05	Asn 120, Thr 215, Ile 125, Asn 91, Ala 167, Phe 142, Thr 147, Lys 168, Ile 141
	Camptothecin	-3.180	-8.871	-1735.960	08	Ile 125, Ser 149, Gly 164, Ser 148, Asn 150, Ala 167, Gly 166
	Salvicine	-34.550	-9.064	-1736.780	03	Ala 32, Asn 91, Ile 88, Ile 217
Control- 2	Daunorubin	-36.326	-6.455	-1748.350	09	Lys 157, Gln 97, Arg 98, Glu 185
Vascular endothelial	Quercetin	-64.420	-12.030	-675.940	08	Glu 883, Lysine 866, Val 846, Ala 864, Leu

growth factor receptor-2						838, Val 914, Glu 915, Phe1045, Phe 916, Asp 1044, Cys 1043, Leu 1033, Cys 917
	Decursinol	-62.710	-9.829	-671.910	04	Leu 838, Val 846, Ala 864, Lys 866, Phe 916, Cys 917, Val 914, Leu 1033, Val 897, Leu 887, Glu 883
	Plumbagin	-48.910	-8.602	-669.000	05	Val 846, Leu 838, Leu 1033, Cys 917, Phe 916, Glu 915, Ala 864
Control- 3	Lenvatinib	-103.24	-13.121	-661.023	09	Asp 1044, Cys 1043, Leu 1033, Cys 917, Lys 918, Phe 916, Glu 915, Val 914, Ala 864, Lys 866, Val 846, Asp 1044, Cys 1043

Name of the ligand (with respective receptor)	Docking Score (Binding Energy) (Kcal/mol)	Interacting amino acids	Bond distance in Å	Interaction category	Type of interaction
Epigallocatechin gallate (cyclin-dependent kinase-2)	-7.341	Lysine 89	1.82	Classical hydrogen bond	Conventional
		Leucine 298	1.53	Classical hydrogen bond	Conventional
		Histidine 84	2.13	Classical hydrogen bond	Conventional
			2.88	Non-classical hydrogen bond	Carbon
		Glutamic acid 08	1.53	Classical hydrogen bond	Conventional
		Isoleucine 10	4.84	Hydrophobic bond	Pi-Alkyl
			5.18	Hydrophobic bond	Pi-Alkyl
		Leucine 134	4.53	Hydrophobic bond	Pi-Alkyl
		Glutamine 131	1.69	Classical hydrogen bond	Conventional
			2.45	Classical hydrogen bond	Conventional
Dadizein (Human topoisomerase II)	-7.855	Asparagine 120	1.76	Classical hydrogen bond	Conventional
		Threonine 215	2.46	Non-classical hydrogen bond	Carbon
		Isoleucine 125	4.79	Hydrophobic bond	Pi-Alkyl
			5.32	Hydrophobic bond	Pi-Alkyl
		Asparagine 91	2.96	Classical hydrogen bond	Conventional
		Alanine 167	4.88	Hydrophobic bond	Pi-Alkyl
		Phenylalanine 142	5.59	Hydrophobic bond	Pi-Pi T-shaped
		Threonine 147	1.70	Classical hydrogen bond	Conventional
		Lysine 168	2.65	Classical hydrogen bond	Conventional
		Isoleucine 141	4.68	Hydrophobic bond	Pi-Alkyl

Quercetin (Vascular Endothelial Growth Factor Receptor-2)	-10.441	Glutamic acid 883	2.69	Classical hydrogen bond	Conventional
		Lysine 866	5.30	Hydrophobic bond	Pi-Alkyl
		Valine 914	4.81	Hydrophobic bond	Pi-Alkyl
		Glutamic acid 915	2.12	Classical hydrogen bond	Conventional
		Phenylalanine 916	2.51	Non-classical hydrogen bond	Carbon
			1.79	Classical hydrogen bond	Conventional
		Cysteine 917	2.39	Classical hydrogen bond	Conventional
		Leucine 1033	5.32	Hydrophobic bond	Pi-Alkyl
			4.63	Hydrophobic bond	Pi-Alkyl
		Cysteine 1043	5.76	Miscellaneous	Pi-Sulfur
		Aspartic acid 1044	2.80	Classical hydrogen bond	Conventional
		Phenylalanine 1045	5.17	Hydrophobic bond	Pi-Pi stacked
		Alanine 864	4.05	Hydrophobic bond	Pi-Alkyl
			4.95	Hydrophobic bond	Pi-Alkyl
		Valine 846	4.49	Hydrophobic bond	Pi-Alkyl
			5.34	Hydrophobic bond	Pi-Alkyl
		Leucine 838	1.72	Classical hydrogen bond	Conventional
			2.91	Hydrophobic bond	Pi-Sigma
			4.93	Hydrophobic bond	Pi-Alkyl

Table 04. The results of docking studies between the three best ligands and their respective receptors, along with their interaction with different types of amino acids and the bonds formed between the ligands and the amino acids.

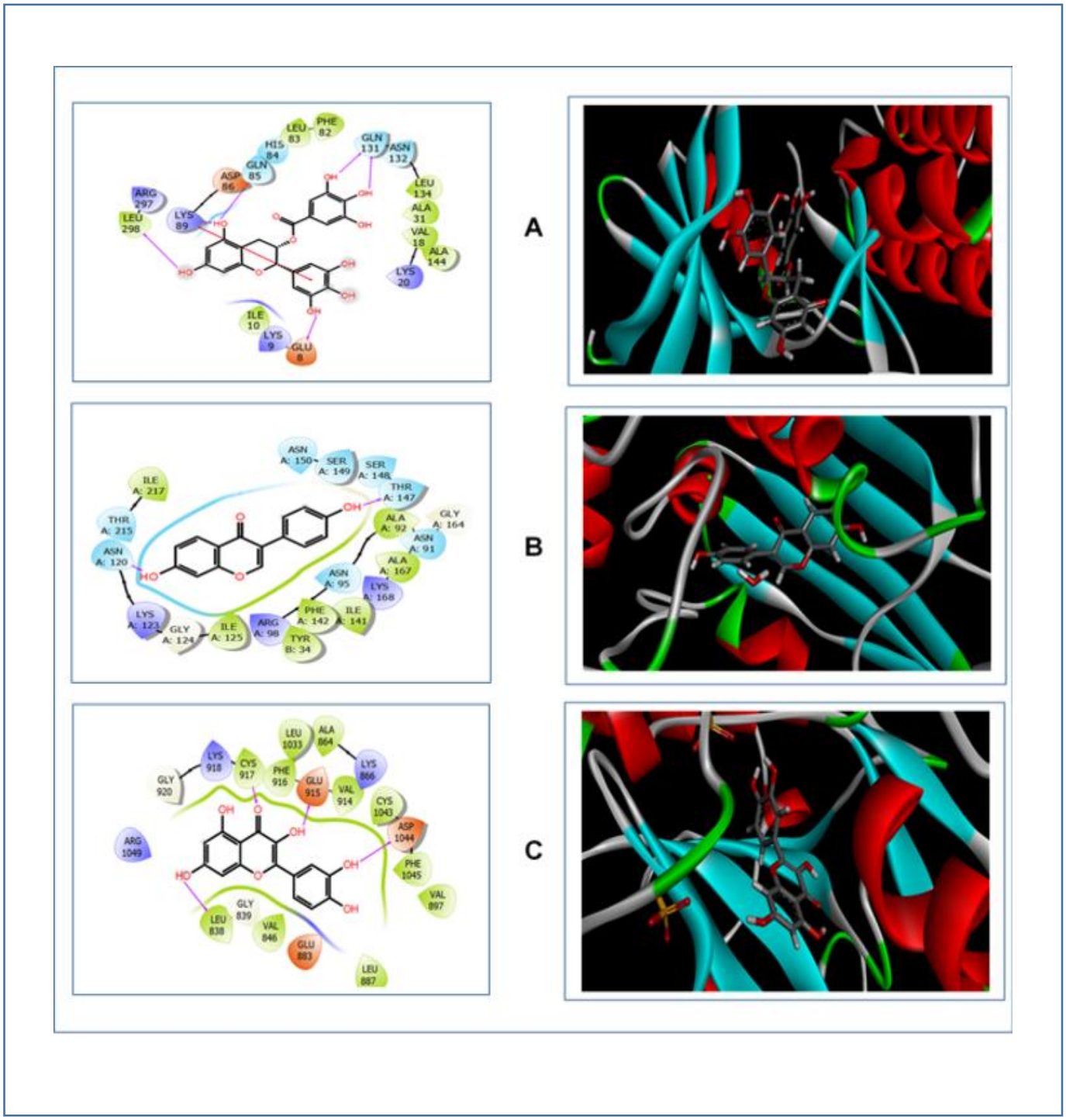
A
B
C

Figure 07. 2D (left) and (3D) representations of the best pose interactions between the three best ligands from each of the enzyme inhibiting group and their respective receptors. A. interaction between epigallocatechin gallate and its receptor cyclin-dependent kinase-2, B. interaction between daidzein and its receptor human topoisomerase II, C. interaction between quercetin and its receptor vascular endothelial growth factor receptor-2. Colored spheres indicates the type of residue in the target: Red-Negatively charged (Asp, Glu), Blue- Polar (His, Gln, Asn, Thr, Ser), Green-Hydrophobic (Ala, Val, Leu, Ile, Phe, Tyr Cys), Light Purple-Basic (Lys, Arg), Gray- Water molecules, Darker gray-metal atom, Light Yellow- Glycine, Deep Purple- Unspecified molecules and the Grayish circles represent Solvent exposure. Interactions are shown as colored lines- Solid pink lines with arrow- H-bond in target (backbone), Dotted pink lines with arrow- H-bond between receptor and ligand (sidechain), Solid pink lines without arrow- Metal co-ordination, Green line- Pi-Pi stacking interaction, Green dotted lines- Distances, Partially blue and red colored lines- Salt bridges. Ligands exposed to solvent are represented by grey sphere. The colored lines show the protein pocket for the ligand according to nearest atom. Interruptions of the lines indicate the opening of the pocket. 2D representations of the best pose interactions between the ligands and their respective receptors were obtained using Maestro-Schrödinger Suite 2018-4. The 3D representations of the best pose interactions between the ligands and their respective receptors were visualized using Discovery Studio Visualizer.

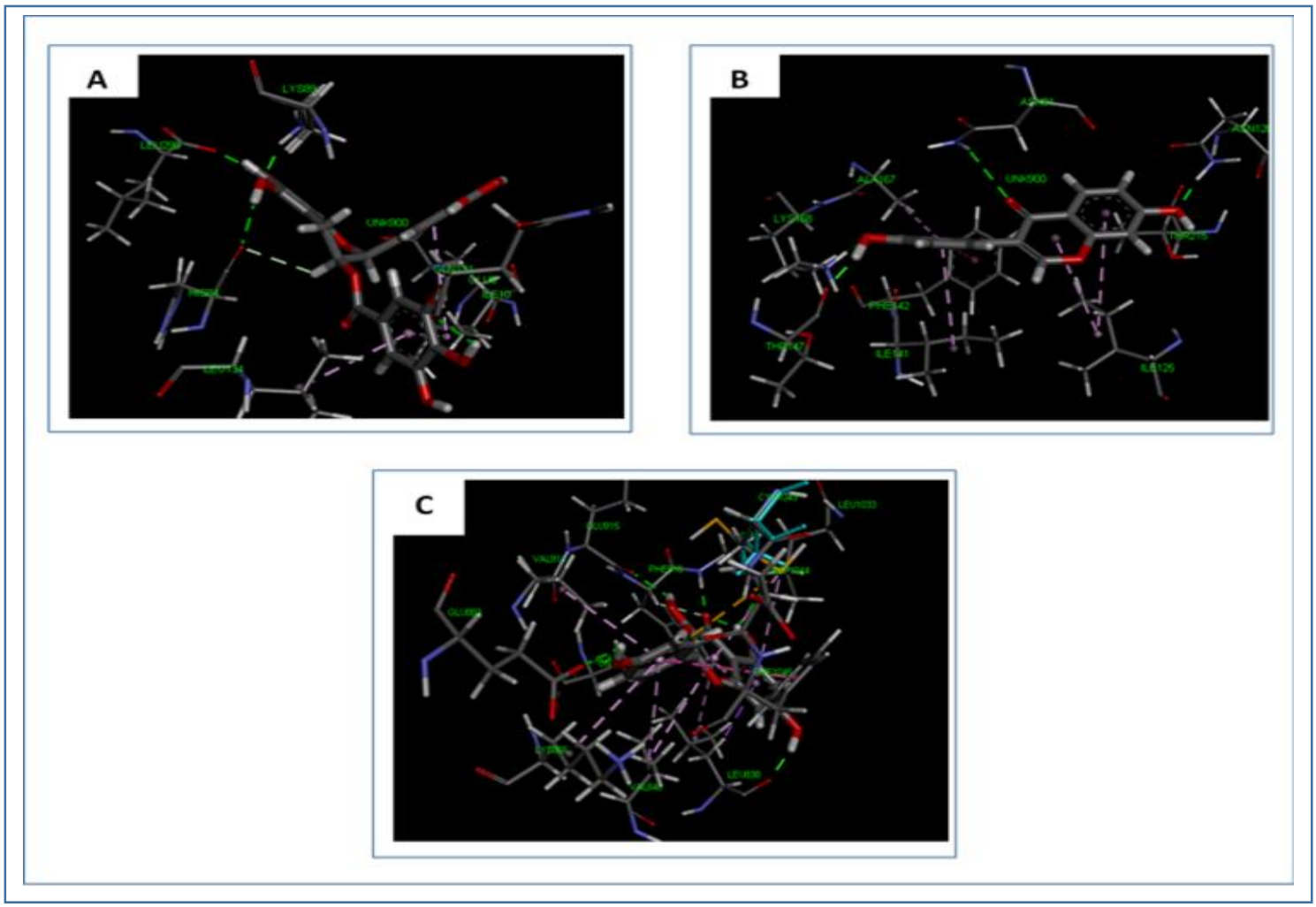

Figure 08. Figure showing the various types of bonds and amino acids that take part in the interaction between the three best selected ligands and their respective receptors. Interacting amino acid residues of target molecule are labeled in the diagram and dotted lines depict interaction between ligand and receptor. Green dotted lines- Conventional bond, Light pink- Alkyl/Pi-Alkyl interactions, Yellow- Pi-Sulfur/Sulphur-X interaction, Deep pink- Pi-Pi stacked bond, Orange- Charge-Charge interaction, Purple- Pi-Sigma interaction, Red- Donor-Donor interaction. A. interaction between epigallocatechin gallate and its receptor cyclin-dependent kinase-2, B. interaction between daidzein and its receptor human topoisomerase II, C. interaction between quercetin and its receptor vascular endothelial growth factor receptor-2. The representations of the interactions between the ligands and the amino acids of the respective receptors were visualized using Discovery Studio Visualizer.

3.2. Druglikeness Properties

Druglikeness property experiments were done for the best three ligand molecules: epigallocatechin gallate, salvicine and quercetin. Among the three ligand molecules, only epigallocatechin gallate violated the Lipinski's rule of five (2 violations) and the other two ligands followed the Lipinski's rule of five. The LogS values of epigallocatechin gallate, daidzein and quercetin were -3.56, -3.53 and -3.16, respectively. Epigallocatechin gallate gave the highest synthetic accessibility (SA) score of 4.20, whereas, daidzein gave SA score of 2.97. Moreover, epigallocatechin gallate had also showed the highest topological polar surface area (TPSA) value of 197.37 $Å^2$ and daidzein showed the lowest TPSA value of 71.97 $Å^2$. Both daidzein and quercetin followed the Ghose, Veber, Egan and muegge rules. However, epigallocatechin gallate didn't follow the Veber, Egan and Muegge rules. Quercetin showed the highest druglikeness score of 1.60 and the lowest score was generated by daidzein (-0.43). The drug scores of epigallocatechin gallate, daidzein and quercetin were 0.7, 0.4 and 0.3, respectively. However, only epigallocatechin gallate showed no reproductive effectiveness and irritant, tumorigenic and mutagenic properties. On the other hand, quercetin showed high tumorigenic and mutagenic properties and daidzein showed high reproductive effectiveness. The results of druglikeness experiments are listed in **Table 05.**

Table 05. The druglikeness properties of the best three ligands. The druglikeness properties were predicted using the SWISSADME server (http://www.swissadme.ch/) and the OSIRIS Property Explorer (https://www.organic-chemistry.org/prog/peo/). Lipinski's rule of five: molecular weight: ≤500, number of hydrogen bond donors: ≤5, number of hydrogen bond acceptors: ≤10, lipophilicity (expressed as LogP): ≤5 and molar refractivity from 40 to 130. Ghose filter factor: logP value between -0.4 and 5.6, molecular weight between 160 and 480, molar refractivity between 40 and 130 and the total number of atoms between 20 and 70. Veber rule: 10 or fewer numbers of rotatable bonds and the polar surface are which should be equal to or less than 140 $Å^2$. Egan rule: the absorption of a candidate drug molecule depends on two factors: the polar surface area (PSA) and AlogP98 (the logarithm of partition co-efficient between n-octanol and water). Muegge rule: a successful drug has to pass a pharmacophore point filter.

Drug Likeness Properties	**Epigallocatechin gallate**	**Daidzein**	**Quercetin**
Molecular weight	458.37 g/mol	254.24 g/mol	302.24 g/mol
Concensus Log $P_{o/w}$	1.01	2.24	1.23
Log *S*	-3.56	-3.53	-3.16
Num. H-bond acceptors	11	4	7
Num. H-bond donors	8	2	5
Molar Refractivity	112.06	71.97	78.03
Lipinski	No (2 violations)	Yes	Yes
Ghose	Yes	Yes	Yes
Veber	No (1 violation)	Yes	Yes
Egan	No (1 violation)	Yes	Yes
Muegge	No (3 violations)	Yes	Yes
Bioavailability score	0.17	0.55	0.55
Synthetic accessibility	4.20	2.79	3.23
TPSA ($Å^2$)	197.37	70.67	131.36
No of rotatable bonds	4	1	1
Druglikeness score	1.58	-0.43	1.60
Drug-Score	0.7	0.37	0.3
Reproductive effective	No	Yes (high)	No
Irritant	No	No	No
Tumorigenic	No	No	Highly tumorigenic
Mutagenic	No	No	Highly mutagenic

3.3 ADME/T Tests

The results of ADME/T test with probability scores are summarized in **Table 06.** In the absorption section, only daidzein showed positive Caco-2 permeability. All the three ligands were p-gp non-substrate and p-gp inhibitor. Moreover, all the three selected ligands were HIA positive. In the distribution section, all the molecules showed high capability to bind with plasma protein (PPB), however, all of them were not blood brain barrier permeable (BBB). In the metabolism section, only epigallocatechin gallate was not inhibitory to CYP450 1A2 and quercetin was the only ligand to inhibit CYP450 3A4. However, only daidzein was not substrate for CYP450 3A4 and the only inhibitor for CYP450 2C9. None of the ligands were substrate for CYP450 2C9 and CYP450 2D6. Moreover, none of them inhibited CYP450 2D6. Only daidzein inhibited CYP450 2C19. The subcellular localization of the three ligands were mitochondria. In the excretion section, epigallocatechin gallate, daidzein and quercetin showed half-life of 1.7, 1.5 and 0.2 h, respectively. Only epigallocatechin gallate showed hERG blocking capability. However, only epigallocatechin gallate didn't show any human hepatotoxic activity (H-HT negative). Only daidzein showed negative result in the Ames mutagenicity test. However, all of them were DILI positive.

Table 06. The ADME/T test results of the best three ligand molecules. The tests were carried out using admetSAR (http://lmmd.ecust.edu.cn/admetsar2/) and ADMETlab servers (http://admet.scbdd.com/).

Class	**Properties**	**Epigallocatechin gallate (with probability)**	**Daidzein (with probability)**	**Quercetin (with probability)**
Absorption	Caco-2 permeability	Negative (0.9372)	Positive (0.931)	Negative (0.6417)
	Pgp-inhibitor	Negative (0.5518)	Negative (0.916)	Negative (0.9191)
	Pgp-substrate	Negative (0.8848)	Negative (0.936)	Negative (0.8360)
	HIA (Human Intestinal Absorption)	Positive (0.9942)	Positive (0.989)	Positive (0.9833)
Distribution	PPB (Plasma Protein Binding)	High, 100%	High, 83.1%	High, 117.06%
	BBB (Blood–Brain Barrier)	Negative (0.5464)	Negative (0.781)	Negative (0.463)
Metabolism	CYP450 1A2 inhibition	Negative (0.805)	Positive (0.910)	Positive (0.910)
	CYP450 3A4 inhibition	Negative (0.766)	Negative (0.626)	Positive (0.695)
	CYP450 3A4 substrate	Positive (0.567)	Negative (0.526)	Positive (0.556)
	CYP450 2C9 inhibition	Negative (0.836)	Positive (0.975)	Negative (0.582)
	CYP450 2C9 substrate	Negative (1.000)	Negative (0.820)	Negative (1.000)
	CYP450 2C19 inhibition	Negative (0.808)	Positive (0.899)	Negative (0.902)
	CYP450 2D6 inhibition	Negative (0.955)	Negative (0.919)	Negative (0.928)
	CYP450 2D6 substrate	Negative (0.721)	Negative (0.800)	Negative (0.855)
	Subcellular localization	Mitochondria	Mitochondria	Mitochondria
Excretion	$T_{1/2}$ (h)	1.7	1.5	0.2
Toxicity	hERG (hERG Blockers)	Blocker (0.812)	Non-blocker (0.394)	Non-blocker (0.371)
	H-HT (Human Hepatotoxicity)	Negative (0.240)	Positive (0.784)	Positive (o.558)
	Ames (Ames Mutagenicity)	Positive (0.560)	Negative (0.184)	Positive (0.740)
	DILI (Drug Induced Liver Injury)	Positive (0.848)	Positive (0.948)	Positive (0.900)

3.4. PASS and P450 Site of Metabolism Prediction

The predicted LD50 value for epigallocatechin gallate, salvicine and quercetin were 1000 mg/kg, 260 mg/kg and 159 mg/kg, respectively. Epigallocatechin gallate showed the toxicity class 4 activity, whereas, salvicine and quercetin were in toxicity class 3.

The prediction of activity spectra for substances (PASS prediction) was for the three selected ligands to identify 20 intended biological activities and 5 adverse & toxic effects. To carry out the PASS prediction experiment, Pa > 0.7 was kept since this threshold give highly reliable prediction (76). The PASS prediction results of all the three selected ligands are listed in **Table 07** and **Table 08.**

The possible sites of P450 metabolism are illustrated in **Table 09.** The possible sites of metabolism by CYPs 1A2, 2A6, 2B6, 2C19, 2C8, 2C9, 2D6, 2E1 and 3A4 of epigallocatechin gallate, daidzein and quercetin were determined. The possible sites of metabolism by the isoforms are indicated by circles on the chemical structure of the molecule (77).

Table 07. The PASS prediction results showing the biological activities of the best three ligand molecules. The tests were carried out using PASS-Way2Drug server (http://www.pharmaexpert.ru/passonline/) kepping Pa> 0.7 as threshold.

Sl no	**Biological activities**	**Epigallocatechin gallate**		**Daidzein**		**Quercetin**	
		Predicted LD50: 1000 mg/kg		**Predicted LD50: 2430 mg/kg**		**Predicted LD50: 159 mg/kg**	
		Toxicity class: 4		**Toxicity class: 5**		**Toxicity class: 3**	
		Pa	**Pi**	**Pa**	**Pi**	**Pa**	**Pi**
01	Antioxidant	0.814	0.003	-	-	0.872	0.003
02	Reductant	0.944	0.002	-	-	-	-
03	Anticarcinogenic	0.841	0.004	-	-	0.757	0.007
04	Antimutagenic	-	-	0.836	0.003	0.940	0.001
05	Chemopreventive	0.860	0.003	-	-	-	-
06	Membrane integrity agonist	0.962	0.003	0.887	0.0014	0.973	0.002
07	Hepatoprotectant	-	-	-	-	0.706	0.007
08	Mucomembranous protector	0.950	0.003	-	-	-	-
09	TP53 expression enhancer	0.937	0.004	0.771	0.014	0.844	0.008
10	Lipid peroxidase inhibitor	0.946	0.002	-	-	-	-
11	HIF1A expression inhibitor	-	-	-	-	0.969	0.002
12	APOA1 expression enhancer	0.856	0.003	-	-	-	-
13	Free radical scavenger	0.934	0.001	-	-	-	-
14	Peroxidase inhibitor	0.759	0.007	-	-	0.962	0.001
15	Oxidoreductase inhibitor	-	-	-	-	-	-
16	CYP1A1 inhibitor	-	-	0.756	0.002	0.909	0.001
17	CYP1A2 inhibitor	-	-	-	-	0.909	0.003
18	Antiviral	0.771	0.003	-	-	-	-
19	Cardioprotectant	-	-	-	-	0.833	0.003
20	Vasoprotector	-	-	0.721	0.009	0.824	0.004

Table 08. The PASS prediction results showing the adverse and toxic effects of the best three ligand molecules. The tests were carried out using PASS-Way2Drug server (http://www.pharmaexpert.ru/passonline/).

Sl no	**Adverse & toxic effects**	**Epigallocatechin gallate**		**Daidzein**		**Quercetin**	
		Pa	**Pi**	**Pa**	**Pi**	**Pa**	**Pi**
01	Inflammation	0.811	0.014	-	-	-	-
02	Toxic, vascular	0.804	0.017	-	-	0.797	0.018
03	Twitching	-	-	-	-	-	-
04	Shivering	-	-	0.783	0.044	0.766	0.052
05	Reproductive dysfunction			-			

Table 09. The P450 site of metabolism prediction of the best three ligand molecules. The prediction was carried out by online server RS-WebPredictor 1.0 (http://reccr.chem.rpi.edu/Software/RS-WebPredictor/). The possible sites of metabolism are marked by circles.

Names of P450 isoenzymes	**Epigallocatechin gallate**	**Daidzein**	**Quercetin**
1A2	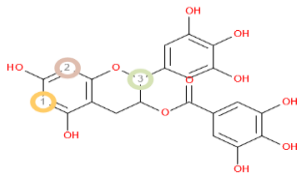	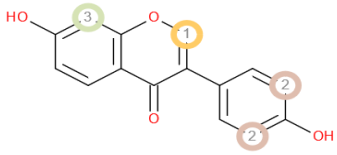	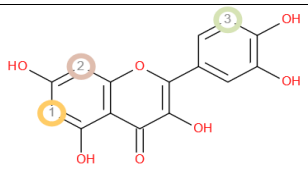
2A6	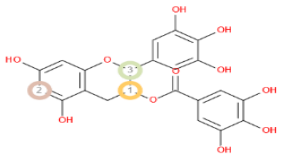	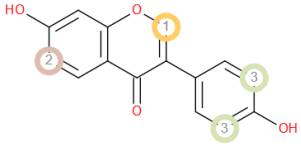	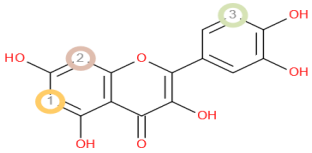
2B6	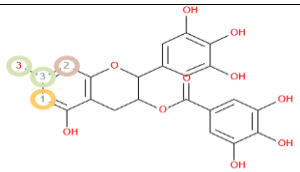	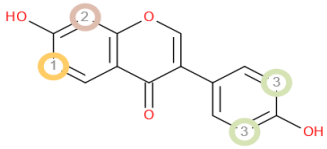	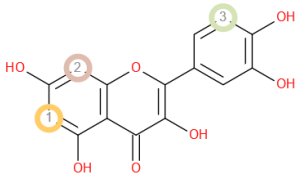
2C8	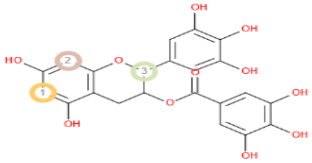	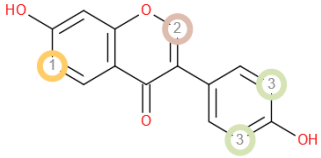	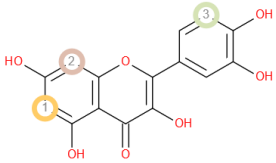

2C9	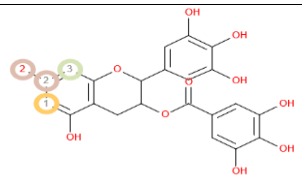	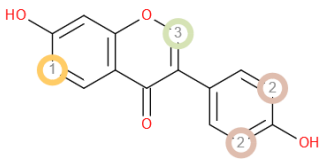	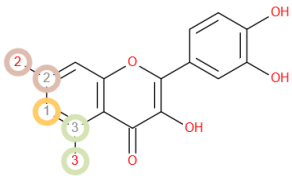
2C19	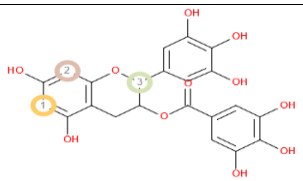	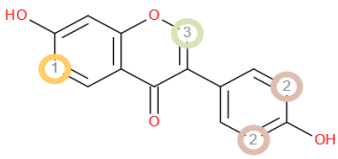	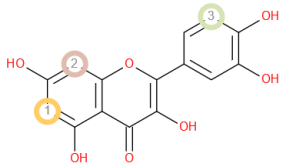
2D6	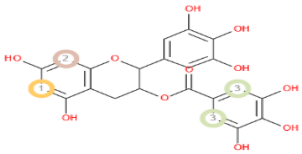	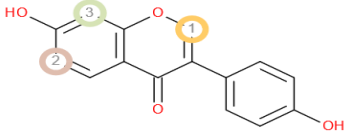	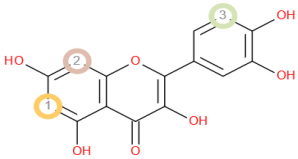
2E1	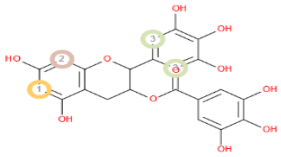	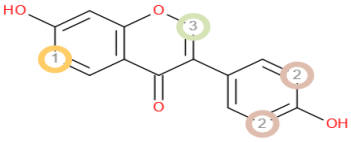	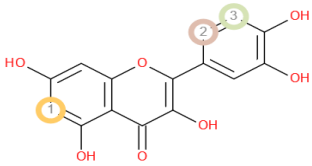
3A4	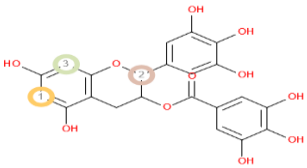	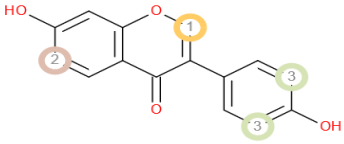	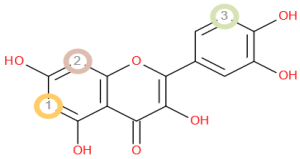

3.5. Pharmacophore Modelling

Both epigallocatechin gallate and daidzein generated 6 point hypothesis and quercetin generated 8 point hypothesis. Epigallocatechin gallate generated 2 hydrogen bonds, 1 pi-cation interaction and 2 bad interactions, daidzein generated only 2 hydrogen bonds and quercetin showed only 1 hydrogen bond with their respective pharmacophores. No ugly contacts were generated by any of the three ligands. However, all of the ligands generated quite a lot good contacts with their respective ligands (**Figure 09**).

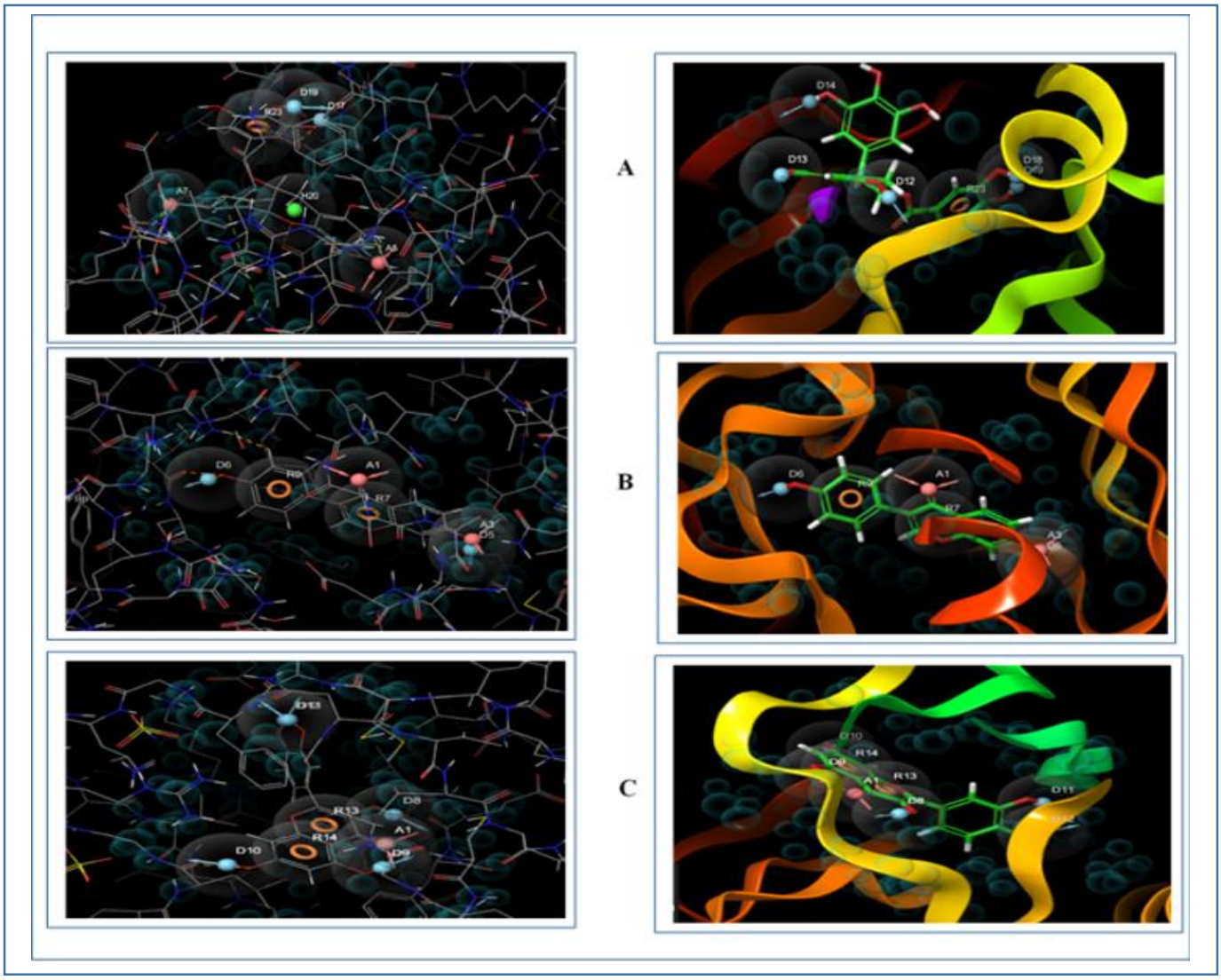

Figure 09. 2D (left) and 3D (right) representations of the pharmacophore modelling of the three best ligand molecules. A. the hypothesis for epigallocatechin gallate and its receptor CDK-2, B. the hypothesis for daidzein and its receptor topoisomerase II, C. the hypothesis for quercetin and its receptor VEGFR-2. The interactions between the ligand and the receptor in the hypothesis were presented by dotted dashed lines, yellow colour- hydrogen bonds and green colour- pi-cation interaction. The bad contacts between the ligands and the pharmacophore are respresented. The pharmacophore modelling was carried out by Maestro-Schrödinger Suite 2018-4.

3.6. Solubility Prediction

All the molecules had the predicted values within the acceptable ranges, except only epigallocatechin gallate, that showed violation in the CIQPlogS value with -6.725 (acceptable range: -6.5- 5). However, epigalloctechin gallate showed the highest QPlogPC16, QPlogPoct and QPlogPo/w values of 10.308, 12.420 and 2.720, respectively. It also had the lowest QPlogS value of -5.797. Daidzein had the highest QPlogPw and CIQPlogS values of 9.963 and -1.787, respectively. Quercetin also showed quite good results in the solubility prediction. The results of solubility prediction are listed in **Table 10**.

Table 10. List of the solubility tests of the three best selected ligands. The tests were carried out by QikPrep wizard of Maestro-Schrödinger Suite 2018-4. Here,

[a]Predicted hexadecane/gas partition coefficient (Acceptable range: 4.0 – 18.0); [b]Predicted octanol/gas partition coefficient (Acceptable range: 8.0 – 35.0); [C]Predicted water/gas partition coefficient (Acceptable range: 4.0 – 45.0); [d]Predicted octanol/water partition coefficient (Acceptable range: –2.0 – 6.5); [e]Predicted aqueous solubility, S in mol dm^{-3} (Acceptable range: –6.5 – 0.5); [f]Conformation-independent predicted aqueous solubility, S in mol dm^{-3}(Acceptable range: –6.5 – 0.5).

Compound Name	**QPlogPC16[a]**	**QPlogPoct[b]**	**QPlogPw[c]**	**QPlogPo/w[d]**	**QPlogS[e]**	**CIQPlogS[f]**
Epigallocatechin gallate	10.308	12.420	5.433	2.720	-5.797	-6.725
Daidzein	5.389	11.284	9.963	0.110	-1.611	-1.787
Quercetin	6.361	9.402	6.934	0.409	-2.498	-3.378

3.7. Analysis of Frontier's Orbitals

In the analysis of Frontier"s orbitals, the DFT calculations and HOMO-LUMO studies were conducted. The results of the DFT calculations are listed in **Table 11**. In these strudies, epigallocatechin gallate showed the lowest gap energy of 0.070 eV as well as the lowest dipole moment of 1.840 debye. Daidzein generated gap energy of 0.080 eV and dipole moment of 3.790 debye. On the other hand, quercetin generated the highest gap energy of 0.167 eV and the highest dipole moment of 5.289 debye. The order of gap energies and dipole moments of these three compounds were, epigallocatechin gallate < daidzein < quercetin (**Figure 10**).

Table 11. The results of the DFT calculations of the selected best three ligands.

Compound name	HOMO energy (eV)	LUMO energy (eV)	Gap (eV)	Hardness (**η**) (eV)	Softness (S) (eV)	Dipole moment (Debye)
Epigallocatechin gallate	0.050	0.120	0.070	0.035	28.571	1.840
Daidzein	-0.040	0.040	0.080	0.040	25.000	3.790
Quercetin	-0.212	-0.045	0.167	0.084	11.904	5.289

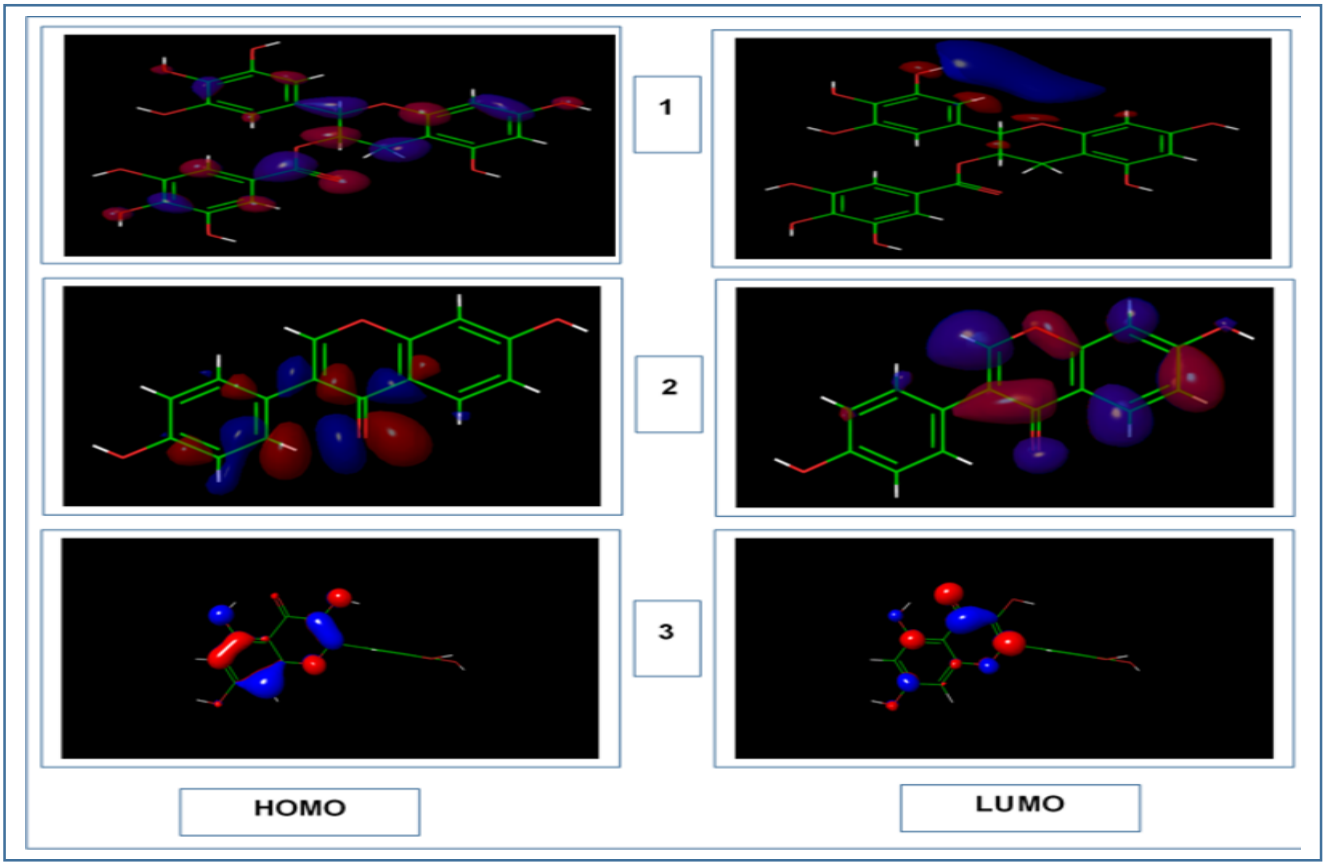

Figure 10. The results of DFT calculations (HOMO-LUMO structures) of, 1. Epigallocatechin gallate, 2. Daidzein and 3. Quercetin.

3.8. Molecular Dynamics Simulation

Figure 11a, **12a** and **13a** illustrate the normal mode analysis (NMA) of epigallocatechin gallate-CDK-2 complex, daidzein-human topoisomerase IIa complex and quercetin-VEGFR-2 complex, respectively. The deformability graphs of the three complexes illustrate the peaks in the graphs correspond to the regions in the protein with deformability (**Figure 11b**, **12b** and **13b**). The B-factor graphs of the complexes give easy visualisation and understanding of the comparison between the NMA and the PDB field of the complexes (**Figure 11c**, **12c** and **13c)**. The eigenvalues of the complexes are illustrated in **Figure 11d**, **12d** and **13d**. Epigallocatechin gallate-CDK-2 complex generated eigenvalue of 8.987362e-04, daidzein-human topoisomerase IIa complex generated eigenvalue of 1.011820e-04 and quercetin-VEGFR-2 complex showed eigenvalue of 1.8912293e-04. The variance graphs indicate the individual variance by red colored bars and cumulative variance by green colored bars (**Figure 11e**, **12e** and **13e**). **Figure 11f**, **12f** and **13f** illustrate the co-variance map of the complexes where the correlated motion between a pair of residues are indicated by red color, uncorrelated motion is indicated by white color and anti-correlated motion is indicated by blue color. The elastic map of the complexes show the connection between the atoms and darker gray regions indicate stiffer regions (**Figure 11g**, **12g** and **13g**) (93, 94, 95).

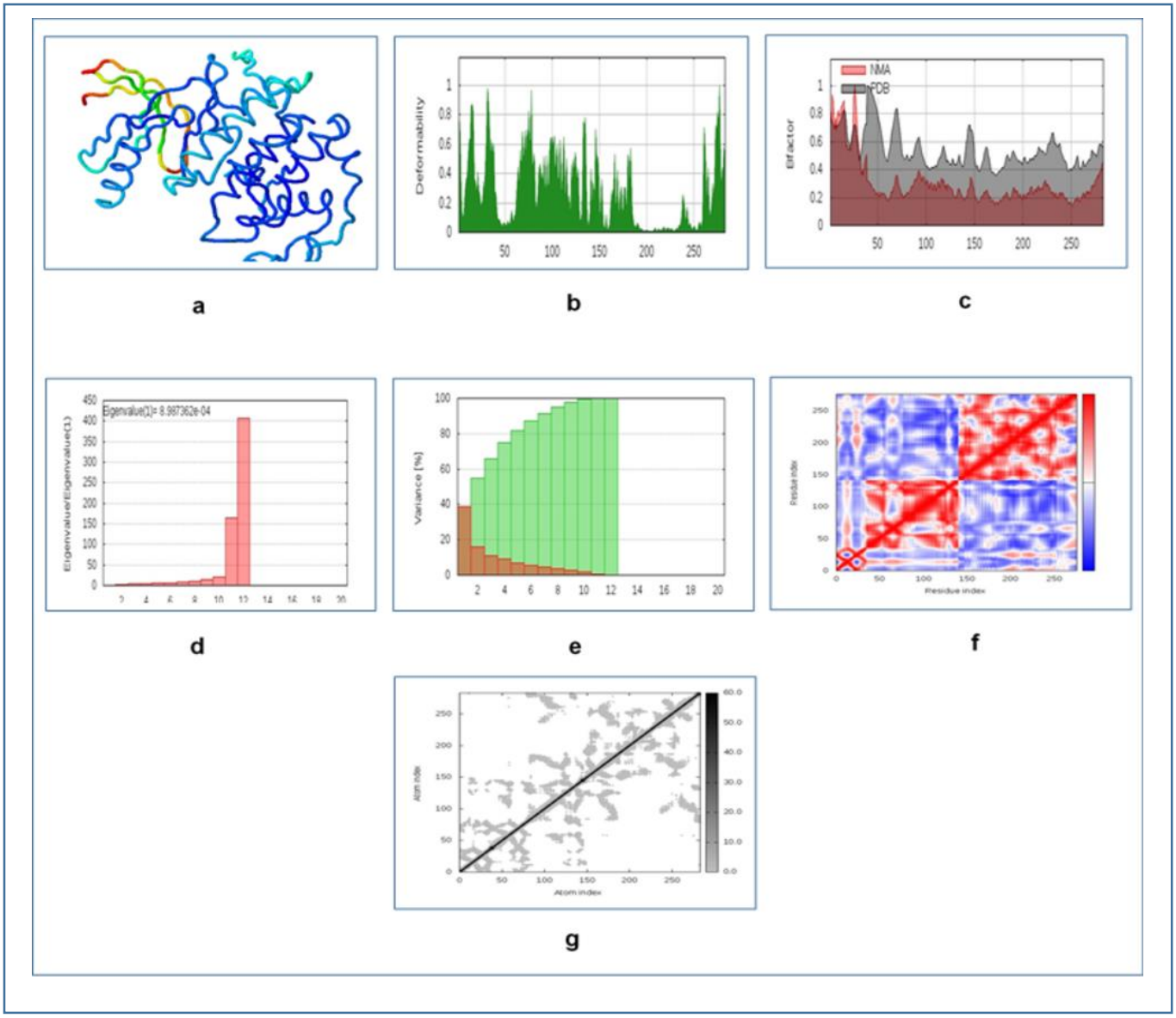

Figure 11. Results of molecular dynamics simulation of epigallocatechin gallate and CDK-2 docked complex. (a) NMA mobility, (b) deformability, (c) B-factor, (d) eigenvalues, (e) variance (red color indicates individual variances and green color indicates cumulative variances), (f) co-variance map (correlated (red), uncorrelated (white) or anti-correlated (blue) motions) and (g) elastic network (darker gray regions indicate more stiffer regions) of epigallocatechin gallate and CDK-2 complex.

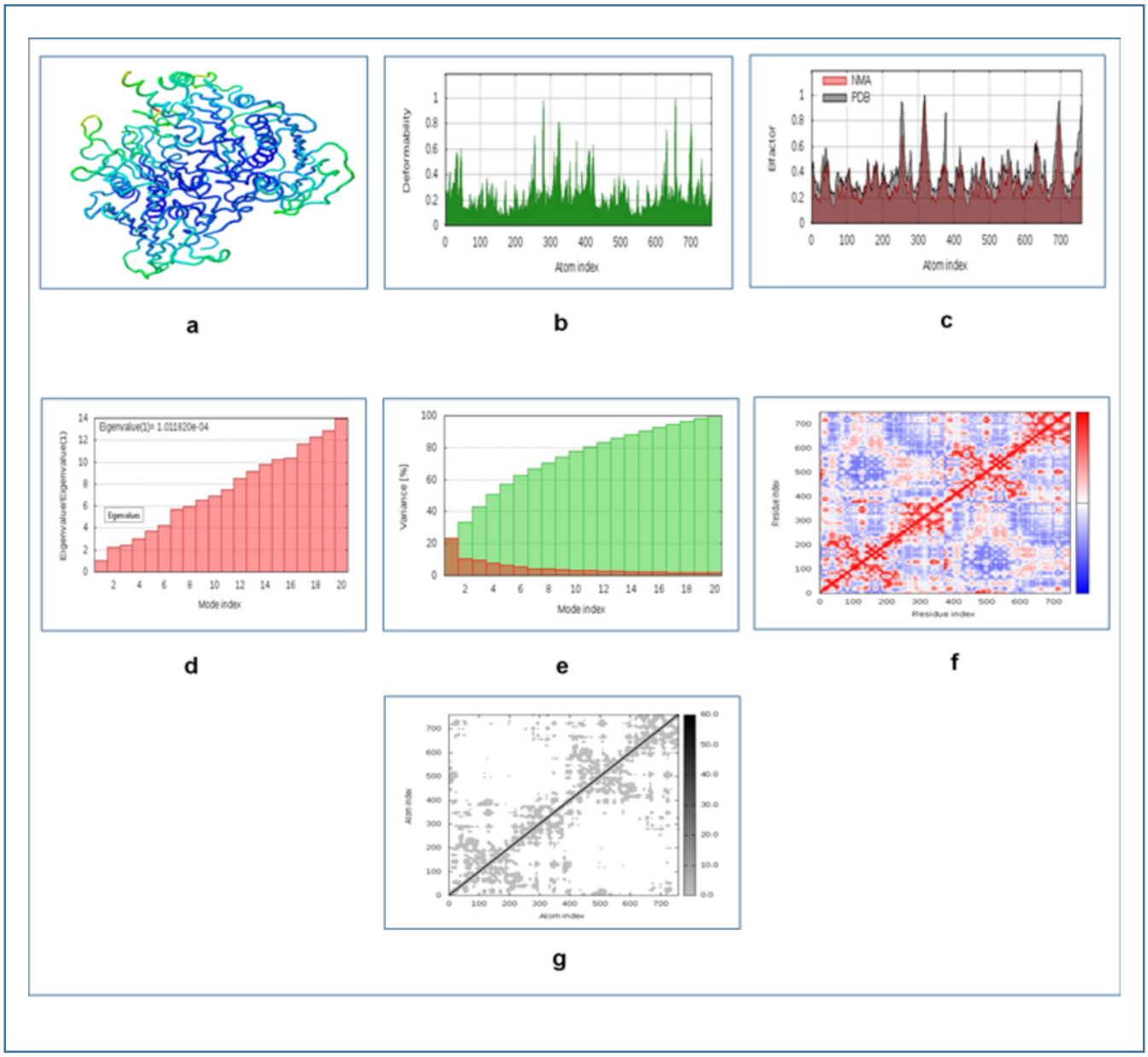

Figure 12. Result of the molecular dynamics simulation of daidzein and human topoisomerase IIa docked complex. (a) NMA mobility, (b) deformability, (c) B-factor, (d) eigenvalues, (e) variance (red color indicates individual variances and green color indicates cumulative variances), (f) co-variance map (correlated (red), uncorrelated (white) or anti-correlated (blue) motions) and (g) elastic network (darker gray regions indicate more stiffer regions) of daidzein and human topoisomerase IIa complex.

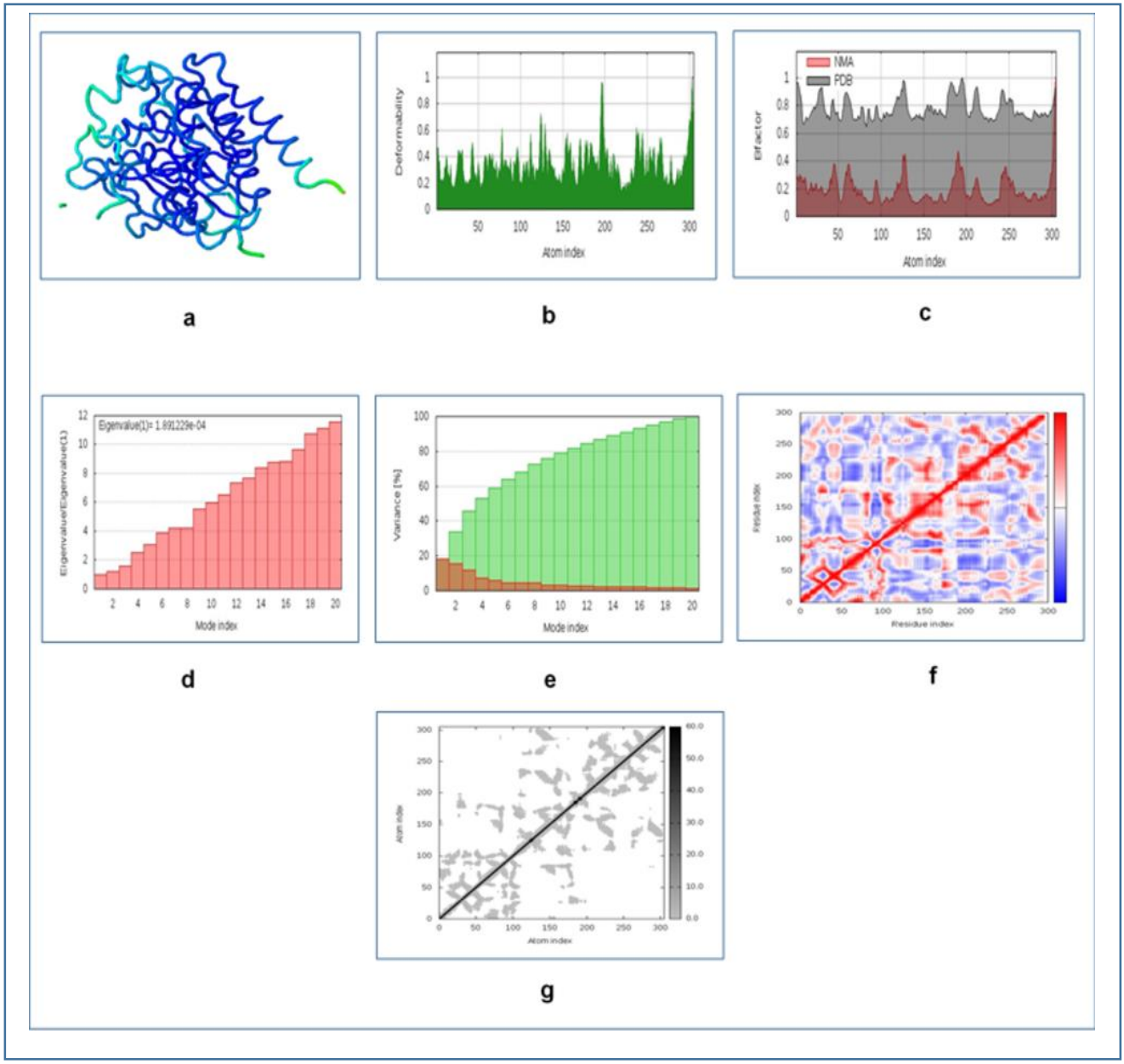

Figure 13. Results of molecular dynamics simulation of quercetin and VEGFR-2 docked complex. (a) NMA mobility, (b) deformability, (c) B-factor, (d) eigenvalues, (e) variance (red color indicates individual variances and green color indicates cumulative variances), (f) co-variance map (correlated (red), uncorrelated (white) or anti-correlated (blue) motions) and (g) elastic network (darker gray regions indicate more stiffer regions) of quercetin and VEGFR-2 complex.

4. Discussion

CDK-2 protein generated excellent Ramachandran plot since it had only a few amino acids in the "allowed" region and almost all of the amino acids in the "favored" region. It had no amino acids in the "disallowed region". Human topoisomerase II also generated good, although not satisfactory results with 15 amino acids in the "disallowed region". It also had majority of the amino acids in the "favored" region. VEGFR-2 generated very good result with only 4 amino acids in the "disallowed" region and most of the amino acids in the "favored" region. The best possible pose of a ligand molecule within the constraint of binding pocket of a receptor molecule is estimated by the processes of molecular docking and thus a binding energy is calculated. The lower the binding energy (docking score), the higher the affinity of binding and vice versa (97, 98, 99). In the experiment, 30 ligand molecules were selected to act against three receptor proteins of three pathways that are responsible for cancer development. Each receptor protein was docked against 10 ligands and from that 10 ligands, one best possible ligand was selected for further analysis. 3 ligands were selected from each group based on the binding energy. Later, from those 3 ligands of each group, one best possible ligand was selected based on MM-GBSA and IFD studies. Therefore, three pathways gave three different possible ligands that were found to be best in inhibiting their receptor proteins.

All the 30 ligands docked successfully with their respective receptors. However, based on the binding energy or docking score (lower score is always preferred), 3 ligands from each of the receptor group (9 ligands in total) were selected: remangiflavanonone B, epigallocatechin gallate, indirubin, daidzein, camptothecin, salvicine, quercetin, decursinol and plumbagin, were selected for MM-GBSA and IFD studies.

In the MM-GBSA and IFD studies, among the three selected ligands from CDK-2 receptor group, epigallocatechin gallate was selected as the best ligand. Although, it had ΔG_{Bind} score of -56.42 Kcal/mol, which was the second lowest ΔG_{Bind} scores among the ligands, it generated XP G_{score} of -8.616 Kcal/mol, which was lowest among the XP G_{scores} generated by the other two ligands and it also generated the lowest IFD score of -594.990 Kcal/mol. For this reason, epigallocatechin gallate was selected as the best ligand among the three ligands that inhibited CDK-2.

Daidzein, camptothecin and quercetin were the three ligands selected in the human topoisomerase II category, based on the docking score. The MM-GBSA and IFD studies indicated that daidzein should be the best ligand among the three selected ligands with the lowest ΔG_{Bind} score and quite good IFD results.

Quercetin, decursinol and plumbagin were the three ligands selected based on the binding energy or docking score, from the VEGFR-2 enzyme category. Since, quercetin generated the lowest as well as the best ΔG_{Bind} score, XP G_{score} and IFD score, it was selected as the best ligand among the three selected ligand molecules. Further analysis were later conducted on epigallocatechin gallate, daidzein and quercetin to determine their safety and efficacy. Among the three best ligands, epigallocatechin gallate showed the highest docking score of -7.341 Kcal/mol, for this reason, it interacted with the least amount of amino acids (7) within the binding pocket of CDK-2. Daidzein has the second lowest docking score of -7.855 Kcal/mol, for this reason it interacted with 9 amino

acids (higher than epigallocatechin gallate, but lower than quercetin) within the binding pocket of its receptor, human topoisomerase II. And since quercetin had the highest docking score against its receptor VEGFR-2, it interacted with the highest number of amino acids (13) (**Table 02, Table 03, Table 04, Figure 07 and Figure 08**).

Comparing with the controls, alvocidib generated the docking score and glide energy which were higher than many of the scores generated by the ligands (inhibited CDK-2). Moreover, epigallocatechin gallate also showed superior results in all the parameters except the MM-GBSA study. For this reason, epigallocatechin gallate could be used effectively in treating cancers inhibiting CDK-2. Furthermore, another control, daunorubicin generated also generated poor results than many of the selected ligands that inhibited human topoisomerase IIa as well as the selected best ligand, daidzein, like epigalloctaechin gallate, showed far better results than daunorubicin in the docking study. For this reason, daidzein can also be used to inhibit human topoisomerase IIa for cancer treatment. However, lenvatinib showed very good performances in the docking study and comparing with lenvatinib, the best selected ligand, quercetin also showed very good results in the docking study, inhibiting VEGFR-2. These three ligands should show good outcome when being used in cancer treatment.

Estimation of the drug likeness properties facilitates the drug discovery and development process. Drug permeability through the biological barrier is influenced by the molecular weight and topological polar surface area (TPSA). The higher the molecular weight and TPSA, the lower the permeability of the drug molecule is and vice versa. Lipophilicity is expressed as LogP. Lipophilicity affects the absorption of the drug molecule in the body. Higher LogP associates with lower absorption and vice versa. LogS value influences the solubility of the target drug molecule and the lowest value is always considered as the best value. The number of hydrogen bond donors and acceptors beyond the acceptable range also affects the capability of a drug molecule to cross the cell membrane. The number of rotatable bonds also affects the druglikeness properties and the acceptable range is less than 10. Moreover, the Lipinski's rule of five demonstrates that a successful drug molecule should have properties within the acceptable range of the five Lipinski's rules: molecular weight: ≤500, number of hydrogen bond donors: ≤5, number of hydrogen bond acceptors: ≤10, lipophilicity (expressed as LogP): ≤5 and molar refractivity from 40 to 130 (105, 106, 107). Moreover, according to the Ghose filter, a candidate drug should have logP value between -0.4 and 5.6, molecular weight between 160 and 480, molar refractivity between 40 and 130 and the total number of atoms between 20 and 70, to qualify as a successful drug (108). Veber rule describes that the oral bioavailability of a candidate drug depends on two factors: 10 or fewer numbers of rotatable bonds and the polar surface are which should be equal to or less than 140 $Å^2$ (109). Furthermore, according to the Egan rule, the absorption of a candidate drug molecule depends on two factors: the polar surface area (PSA) and AlogP98 (the logarithm of partition co-efficient between n-octanol and water) (110). And according to the Muegge rule, for a drug like chemical compound to become a successful drug, it has to pass a pharmacophore point filter, which was developed by the scientists (111). The synthetic accessibility (SA) score evaluates or estimates, how easily a target compound can be synthesized. The score 1 represents very easy to synthesize, whereas, the score 10 represents very hard to synthesize (112). The bioavailability score describes the permeability and bioavailability properties of a possible drug molecule (113).

The druglikeness property experiment showed that only epigallocatechin gallate violated the Lipinski's rule of five (2 violations). It had 8 hydrogen bond donors and 11 hydrogen bond acceptors, which were greater than the required amount of hydrogen bond donors and acceptors of Lipinski's rule of five. The other two molecules had hydrogen bond donors and acceptors within the range required by Lipinski's rule of five. Epigallocatechin gallate had molecular weight of 458.37 g/mol and TPSA of 197.37 $Å^2$. However, daidzein and quercetin had molecular weights of 254.24 g/mol and 302.24 g/mol, respectively and TPSA of 71.97 and 131.26 $Å^2$, respectively. Due to the high molecular weight and TPSA of epigallocatechin gallate, it is relatively less permeable through the biological barrier, whereas, daidzein and quercetin showed good permeability through the biological barrier. Daidzein and quercetin had relatively lower molecular weight and TPSA than epigallocatechin gallate. Epigallocatechin gallate had LogP value of 1.01, for this reason it should be absorbed well in the body. However, due to the highest LogP value of daidzein of 2.24, it should be absorbed less in the body. However, quercetin had LogP value of 1.23, for this reason it should be moderately absorbed by the body. Daidzein and epigallocatechin gallate had almost similar LogS values of -3.53 and -3.56, which indicated that they should have good solubility. However, quercetin, with its LogS value of -3.16, should be less soluble (**Table 05**).

All the selected ligands obeyed the Ghose filter rule. However, only epigallocatechin gallate violated the Veber, Egan and Muegge rules, which also affected the druglikeness properties of epigallocatechin gallate. Epigallocatechin gallate showed bioavailability score of 0.17 and both salvicine and quercetin showed bioavailability score of 0.55. The synthetic accessibility (SA) score of epigallocatechin gallate was 4.20, meaning that it was very had to synthesize. The SA score of daidzein was 2.79, which indicated that it was also relatively easy to synthesize. However, quercetin showed SA score of 3.23 and it should be quite easy to synthesize. Epigallocatechin gallate, daidzein and quercetin had rotatable bonds within the acceptable range of less than 10. The druglikeness score of 1.58 and drug score of 0.7 of epigallocatechin gallate showed that it should be a good drug to treat cancer by repressing CDK-2. Quercetin also had good druglikeness score of 1.60, whereas, its drug score was also not satisfactory (0.3). Daidzein had druglikeness score of -0.43 and drug score of 0.4, which were not satisfactory. Epigallocatechin gallate didn't show any reproductive effectiveness, irritation, tumorigenic and mutagenic properties, whereas, quercetin was highly tumorigenic and mutagenic. On the other hand, only daidzein was highly reproductive effective (**Table 05**).

Considering all the aspects, both epigallocatechin gallate and salvicine should be very good drugs to inhibit their respective targets. Quercetin should also a good drug to inhibit its target VEGFR-2, however, with its high tumorigenic and mutagenic activities, its performances were not quite satisfactory enough to declare it as a very good drug.

The main purpose of conducting ADME/T tests is to determine the pharmacological and pharmacodynamic properties of a candidate drug molecule within a biological system. Therefore, it is a crucial determinant of the success of a drug R&D. Blood brain barrier (BBB) is the most important factor for those drugs that target primarily the brain cells. Most of the drugs are administered through the oral route. For this reason, it would be appreciable that the drug is highly absorbed in intestinal tissue. P-glycoprotein in the cell membrane aids in transporting many drugs,

therefore, its inhibition affects the drug transport. Caco-2 cell line is utilized in in vitro study of drug permeability tests and therefore, its permeability indicates that the drug is easily absorbed in the intestine. Orally absorbed drugs travel through the blood circulation and deposit back to liver and are degraded by group of enzymes of Cytochrome P450 family and excreted as bile or urine. Therefore, inhibition of any of these enzymes of these enzymes affects the biodegradation of the drug molecule (114, 115). Moreover, if a compound is found to be substrate for one or more CYP450 enzyme or enzymes, then that compound is metabolized by the respective CYP450 enzyme or enzymes (116). A drug's proficiency and pharmacodynamics are depended on the degree of its binding with the plasma protein. A drug can cross the cell layers or diffuse easily if it binds to the plasma proteins less efficiently and vice versa (117). Human intestinal absorption (HIA) is a crucial process for the orally administered drugs. The HIA depicts the absorption of orally administered drugs from the intestine into the bloodstream (118, 119, 120). Moreover, The greater the half-life of a drug, the longer the drug would stay in the body and the greater its potentiality, for this reason, half-life determines the doses of drugs (121, 122, 123). HERG is a K^+ channel found in the heart muscle which mediates the correct rhythm of the heart. Blocking the hERG signaling can lead to the cardiac arrhythmia and sometimes death (124, 125). Human liver is the main site of metabolism and it is extremely vulnerable to the harmful effects of various drugs and xenobiotic agents. Human hepatotoxicity (H-HT) involves any type of injury to the liver that may lead to organ failure and even death (126, 127). Ames test is a mutagenicity assay that is used to detect the potential mutagenic chemicals (128). Drug induced liver injury (DILI) is the injury to the liver that are caused by administration of drugs. DILI is one of the causes that causes the acute liver failure (129). The results of ADME/T test are listed in **Table 06.**

In the absorption section of ADME/T test, epigallocatechin gallate and quercetin showed similar performances. Their absorption capability was quite poor since they exhibited Caco-2 impermeability and p-gp inhibitory activity. However, they showed positive result in the human intestinal absorption activity. In the absorption test, daidzein showed better performance than the other two ligands, since it had Caco-2 permeability and human intestinal absorption capability. In distribution section, all of the ligands had similar performance with high plasma protein binding ability and blood brain barrier impermeability. In the metabolism section, daidzein showed the worst performance among the three ligands, since it was not substrate for any of the isoenzymes as well as it showed inhibitory activities on CYP450 1A2, Cyp450 2C9 and CYP450 2C19. Epigallocatechin gallate was non-inhibitor for all of the isoenzymes and only substrate for CYP450 3A4. Quercetin was the inhibitor of CYP450 1A2 and CYP450 3A4, however, it was substrate for only CYP450 3A4. All the three ligands had subcellular localization of mitochondria. In the metabolism section, epigallocatechin gallate showed the best performance among the three ligands. In the excretion section, daidzein had the half-life value of 1.5 h, followed by quercetin with 1.7 h. Quercetin was the poorest performer in the excretion section. In the toxicity section, both daidzein and quercetin performed quite similarly. They were hERG non-blockers and human hepatotoxic, however, only daidzein wes not Ames mutagenic and all of them were DILI positive. Quercetin was the most toxic among the three ligands since it was human hepatotoxic, Ames mutagenic and DILI positive, although it was not hERG blocker. In the ADME/T test, both epigallocatechin gallate and quercetin performed quite similarly. However, daidzein, with its best performance, was found to be more effective than the other two ligands.

Prediction of Activity Spectra for Substances or PASS prediction is a process that is used to estimate the possible profile of biological activities associated with drug-like molecules. Two parameters are used for the PASS prediction: Pa and Pi. The Pa is the probability of a compound "to be active" and Pi is the probability of a compound "to be inactive" and their values can range from zero to one (80). If the value of Pa is greater than 0.7, the probability of exhibiting the activity of a substance in an experiment is higher. However, if the Pa is greater than 0.5 but less than 0.7, the probability of exhibiting a particular activity in an experiment is good, although less than the activity determined when Pa > 0.7 threshold is used. And if Pa is less than 0.5, then the probability of exhibiting the activity is the least (130). The chance of finding any given activity in an experiment increases with the increasing value of Pa and decreasing value of Pi (80). PASS was predicted for epigallocatechin gallate, salvicine and quercetin. The PASS prediction was perfromed for 20 intended biological activities and 5 adverse and toxic effects at Pa > 0.7 threshold. Epigallocatechin gallate showed 12 biological activities and only 2 adverse and toxic effects: inflammation and vascular toxicity. However, daidzein showed 5 biological activities and it showed only 1 adverse effect. On the other hand, quercetin showed 12 biological activities and 2 toxic effects (**Table 07 and Table 08**). However, epigallocatechin gallate and quercetin performed similarly in the PASS prediction test and showed a good number of beneficial biological effects.

ProTox-II server estimates the toxicity of a chemical compound and classifies the compound into a toxicity class ranging from 1 to 6. The server classifies the compound according to the Globally Harmonized System of Classification and Labelling of Chemicals (GHS) (83). According to the Globally Harmonized System of Classification and Labelling of Chemicals (GHS), Class 1: fatal if swallowed (LD50 ≤ 5), class 2: fatal if swallowed (5 < LD50 ≤ 50), class 3: toxic if swallowed (50 < LD50 ≤ 300), class 4: harmful if swallowed (300 < LD50 ≤ 2000), class 5: may be harmful if swallowed (2000 < LD50 ≤ 5000) (131). And ProTox-II server adds one more class to the 5 classes, making them 6 classes in total, class VI: non-toxic (LD50 > 5000) (http://tox.charite.de/protox_II/index.php?site=home) (83). The predicted LD50 value of epigallocactechin gallate was 1000 mg/kg and predicted toxicity class was 4. The toxicity class 4 describes that if a compound is found to be in toxicity class 4, it would be harmful if swallowed. For this reason, epigallocatechin gallate would be harmful if swallowed. Daidzein showed predicted LD50 2430 mg/kg and predicted toxicity class: 5. For this reason, daidzein might be harmful if swallowed. And the predicted LD50 value for quercetin was 159 mg/kg and the predicted toxicity class was 3. Due to the class 4 toxicity level, quercetin would also be toxic if swallowed.

The Cytochrome P450 (Cyp450) is a superfamily of enzymes that comprises of 57 isoforms of P450 enzymes. These enzymes are heme-containing enzymes and they catalyze the phase-I metabolism of almost 90% of the marketed drugs (132). These enzymes catalyzes the conversion of the lipophilic drugs to more polar compounds and for this reason, the kidney can excrete them easily (133). Among the 57 isoforms, nine most prevalent isoforms are: CYPs 1A2, 2A6, 2B6, 2C19, 2C8, 2C9, 2D6, 2E1 and 3A4. The Sites of Metabolism (SOMs) of nine isoforms a specific drug molecule can be determined by an online tool RS-WebPredictor. The possible sites of metabolism by the isoforms are indicated by spherical circles on the chemical structures of the molecules (82). The results of P450 SOM are listed in **Table 09.** Epigallocatechin gallate showed,

3 SOMs for CYP450 1A2, CYP450 2A6, CYP450 2C8, CYP450 2C19 and CYP450 3A4, 4 SOMs for CYP450 2B6, CYP450 2C9, CYP450 2D6, CYP450 2E1. Moreover, daidzein showed 4 SOMs for all the CYP450 isoenzymes. On the other hand, quercetin had 5 SOMs for only CYP450 2C9 isoenzyme and 3 SOMs for the other isoenzymes. Now, considering the P450 study, it can be concluded that daidzein had the best performance in the P450 SOM prediction experiment, since it had 4 SOMs for almost all the isoenzymes and 5 SOMs for CYP450 2B6 and CYP450 2C8 isoenzymes. For this reason, it would be metabolized by the isoenzymes quite well. Epigallocatechin gallate also showed quite good result in the CYP450 SOM prediction, however, quercetin showed poor performance among the three ligands, in the test. For this reason, quercetin would be metabolized less efficiently than the other two molecules. However, all the three molecules should be metabolized quite efficiently by the CYP450 isoenzymes.

The Phase pharmacophore perception is a tool of Maestro-Schrödinger Suite 2018-4 which is used in pharmacophore modelling, QSAR model development and screening of 3D database. The engine provides 6 types of built-in features and the pharmacophore modelling is mainly done based on these 6 types of features: hydrogen bond acceptor (A), hydrogen bond donor (D), negative ionizable (N), positive ionizable (P), hydrophobe (H), and aromatic ring (R). However, the feature number can be increased by customization. The pharmacophore modelling generates a hypothesis which can be used successfully in biological screening for further experiments (134). All the three best ligand molecules successfully generated the pharmacophore modelling hypothesis with their respective targets. In generating the hypothesis, 6 features were selected for epigallocatechin gallate, 6 features were selected for daidzein and 8 features were selected for quercetin. For this reason, both epigallocatechin gallate and daidzein showed 6 point hypothesis and quercetin showed 3 point hypothesis. All the ligands generated quite good hypothesis with their respective receptors. Since, all the ligands formed good hypotheses with their respective pharmacophores, all of the hypotheses can be used in screening (**Figure 09**).

All the ligands generated successful solubility results in the solubility test. The acceptable range for QPlogPC16 is 4.0 – 18.0, the acceptable range for QPlogPoct is 8.0 – 35.0, the acceptable range for QPlogPw is 4.0 – 45.0, the acceptable range for QPlogPo/w is -2.0 – 6.5, the acceptable range for QPlogS is –6.5 – 0.5, the acceptable range for CIQPlogS is –6.5 – 0.5 (135). Both daidzein and quercetin showed very good results in the solubility tests with values well within the acceptable ranges. However, only epigallocatechin gallate generated CIQPlogS score of -6.725, which was not in the acceptable range. However, it also performed quite well in the other parameters **(Table 10).**

Frontier orbitals study or DFT calculation is an essential method of determining the pharmacological properties of various small molecules. HOMO and LUMO help to study and understand the chemical reactivity and kinetic stability of small molecules. The term 'HOMO' directs to the regions on a small molecule which may donate electrons during a complex formation and the term 'LUMO' indicates the regions on a small molecule that may receive electrons from the electron donor(s). The difference in HOMO and LUMO energy is known as gap energy. Gap energy corresponds to the electronic excitation energy. The compound that has the greater orbital gap energy, tends to be energetically unfavourable to undergo a chemical reaction and vice versa.

Moreover, the HOMO-LUMO gap also has correlation with the hardness and softness of a molecule (88, 136, 137, 138, 139). Epigallocatechin gallate showed the lowest gap score of 0.070 eV than daidzein and quercetin, for this reason, epigallocatechin gallate is energetically more favourable to undergo chemical reactions than daidzein. Moreover, the lowest gap scores also corresponds to lowest hardness score and the highest softness score of epigallocatechin gallate, 0.035 eV and 28.571 eV, respectively. However, quercetin generated the highest dipole moment score of 5.289 debye (**Table 11** and **Figure 10**).

The molecular dynamics study and normal mode analysis are carried out to determine the stability and mobility of protein complexes. From the deformability graphs of the protein complexes, it is clear that, epigallocatechin gallate-CDK-2 complex had greater degree of deformability than the other two complexes (**Figure 11b**, **12b** and **13b**). Daidzein-human topoisomerase IIa complex gave the best result in B-factor test since it had lower differences between the NMA and PDB fields among the three complexes (**Figure 11c**, **12c** and **13c).** However, with the highest eigenvalue of 8.987362e-04, epigallocatechin gallate-CDK-2 complex is much harder to deform than the other two complexes (**Figure 11d**, **12d** and **13d).** Quite similar performances were shown by the three complexes in the variance study (**Figure 11e**, **12e** and **13e).** The covariance map indicates coupling between pairs of residues and the graphs indicate strong correlated motions (indicated by red color) of the residues in all the complexs with lesser amount of un-correlated (indicated by white color) and anti-correlated (indicated by blue color) motions between the paired residues (**11f**, **12f** and **13f).** Similar performances were also generated in the elastic network experiment with a lot of stiffer regions (indicated by darg ray color) (**Figure 11g**, **12g** and **13g)** (91, 92, 93, 94, 95). The performances of daidzein-human topoisomerase IIa complex and quercetin-VEGFR-2 complexes were quite similar and all the three complexes showed average results in the molecular dynamics simulation study.

Considering all the aspects, all the three best ligands showed quite good results in the molecular docking study, when compared with their respective controls. Daidzein generated the best results in almost all the tests while inhibiting human topoisomerase IIa. Quercetin also showed quite good results in the tests while inhibiting VEGFR-2, however, the results of epigallocatechin gallate were not quite satisfactory like the other two ligands, while inhibiting the CDK-2. Although, all of the three ligands were found to be quite similarly potential and effective, however, only daidzein could be concluded as the safest agent for the humans. However, these three ligands could be effectively used to treat cancer by their respective pathways. Various in vitro studies had also confirmed this claim. The CDK-2 inhibitory effects of epigalloctaechin gallate were tested on 3T3-L1 preadipocytes, where the preadipocytes were treated with epigallocatechin gallate for 48 hours and it showed reduction of the protein level and inhibition of the activity of CDK-2 in a dose dependent manner (140). The inhibitory activity of daidzein on human topoisomerase II was demonstrated by scientists where ethanolic extract containing daidzein from *Psoralea corylifolia* was used on SV40 infected monkey kidney cells. In the experiment, daidzein showed inhibitory effects towards the topoisomerase II along with DNA polymerase (30). Moreover, daidzein also showed DNA topoisomerase II inhibitory activity when tested on the chinese hamster V79 cells (141). On the other hand, inhibitory activities of quercetin on angiogenesis via suppressing VEGFR-2 pathway had been reported in several studies (43, 142, 143). Epigallocatechin gallate can be extracted from

Camellia sinensis, daidzein can be extracted from many plants of the psoralea species as well as in many non-legume plants and quercetin is a widely available agent found in plants like *Morus alba*, *Camellia sinensis*, *Allium cepa*, *Malus domestica*, *Conriandrum sativum* etc. (144, 145, 146, 147). For this reason, these plants can be considered as potential anti-cancer plants and could be used to treat cancers.

5. Conclusion

In the experiment, 30 anti-cancer agents were selected to analyse against three enzymes, CDK-2, human topoisomerase IIa and VEGFR-2, of three different pathways that lead to cancer development. 10 ligands were studied for each of the enzyme gropu using various tools of in silico biology. From the three groups of enzymes of receptors, epigallocatechin gallate (receptor: CDK-2), daidzein (receptor: human topoisomerase IIa) and quercetin (VEGFR-2), were found to be the best ligands that have the potentiality to inhibit cancer progression. All of them had quite similar potentiality and efficacy, however, epigallocatechin gallate and quercetin were found to be less safe than daidzein for human treatment. However, more in vivo and in vitro researches should be performed on these agents as well as the other remaining agents to finally confirm their potentiality, safety and efficacy.

6. Acknowledgements

Authors are thankful to Swift Integrity Computational Lab, Dhaka, Bangladesh, a virtual platform of young researchers, for providing the tools.

7. Conflict of interest

Bishajit Sarkar declares that he has no conflict of interest. Md. Asad Ullah declares that he has no conflict of interest. Syed Sajidul Islam declares that he has no conflict of interest.

References

1. World health statistics 2006. **2006**, 1–80, WHO (http://www.who.int/)
2. Da, Rocha., A.B., Lopes, R.M. and Schwartsmann, G. Natural products in anticancer therapy. *Curr. Opin. Pharmacol.* ***2001***, *1*(4), 364-369.
3. Cragg, G., M.; Newman, D., J. Plants as a source of anti-cancer agents. *J. Ethnopharmacol.* ***2005***, *100*(1-2), 72-79.
4. Pan, L.; Chai, H.; Kinghorn, A., D. The continuing search for antitumor agents from higher plants. *Phytochem. Lett*. **2010**, *3*(1), 1-8.
5. Sarkar, B.; Ullah, M., A.; Islam, M., S.; Hossain, S; Nafi-Ur-Rahman, M. Anticancer potential of medicinal plants from Bangladesh and their effective compounds against cancer. *J. Pharmacogn. Phytochem.* 2019, *8*(3), 827-833.
6. Pan, L.; Chai, H., B.; Kinghorn, A., D. Discovery of new anticancer agents from higher plants. *Front. Biosci. (Scholar edition)* **2012,** *4*, 142.
7. Fischbach, M., A.; Walsh, C., T. Directing biosynthesis. *Science* **2006**, *314*(5799), 603-605.
8. Fabricant, D., S.; Farnsworth, N., R. The value of plants used in traditional medicine for drug discovery. *Environ. Health Persp.* **2001**, *109*(suppl 1), 69-75.
9. Tan, G.; Gyllenhaal, C.; Soejarto, D., D. Biodiversity as a source of anticancer drugs. *Curr. Drug Targets* **2006**, *7*(3), 265-277.
10. Saklani, A.; Kutty, S., K. Plant-derived compounds in clinical trials. *Drug Discov. Today* **2008**, *13*(3-4), 161-171.
11. Khan, W.; Ashfaq, U., A.; Aslam, S.; Saif, S.; Aslam, T.; Tusleem, K.; Maryam, A.; ul-Qamar, M., T. Anticancer screening of medicinal plant phytochemicals against Cyclin-Dependent Kinase-2 (CDK2): An in-silico approach. *Adv. Life Sci.* **2017**, *4*(4), 113-119.
12. Amin, A.; Gali-Muhtasib, H.; Ocker, M.; Schneider-Stock, R. Overview of major classes of plant-derived anticancer drugs. *Int. J. Biomed. Sci.* **2009**, *5*(1), 1.
13. Ramirez-Mares, M., V.; Chandra, S.; de-Mejia, E., G. In vitro chemopreventive activity of Camellia sinensis, Ilex paraguariensis and Ardisia compressa tea extracts and selected polyphenols. *Mutat. Res.* **2004**, *554*(1-2), 53-65.
14. Ponnusamy, K.; Petchiammal, C.; Mohankumar, R.; Hopper, W. In vitro antifungal activity of indirubin isolated from a South Indian ethnomedicinal plant Wrightia tinctoria R. Br. *J. Ethnopharmacol.* **2010**, *132*(1), 349-354.
15. Jautelat, R.; Brumby, T.; Schäfer, M.; Briem, H.; Eisenbrand, G.; Schwahn, S.; Krüger, M.; Lücking, U.; Prien, O.; Siemeister, G. From the insoluble dye indirubin towards highly active, soluble CDK2-inhibitors. *ChemBioChem*. **2005**, *6*(3), 531-540.
16. K-Jain, S.; B-Bharate, S.; a-Vishwakarma, R. Cyclin-dependent kinase inhibition by flavoalkaloids. *Mini-rev. Med. Chem.* **2012**, *12*(7), 632-649.
17. Lu, X.; Jung, J., I.; Cho, H., J.; Lim, D., Y.; Lee, H., S.; Chun, H., S.; Kwon, D., Y.; Park, J., H. Fisetin inhibits the activities of cyclin-dependent kinases leading to cell cycle arrest in HT-29 human colon cancer cells. *J. Nutr.* **2005**, *135*(12), 2884-2890.
18. Shukla, S.; Gupta, S.; Apigenin-induced cell cycle arrest is mediated by modulation of MAPK, PI3K-Akt, and loss of cyclin D1 associated retinoblastoma dephosphorylation in human prostate cancer cells. *Cell cycle* **2007**, *6*(9), 1102-1114.

19. Lin, Y.; Shi, R.; Wang, X.; Shen, H., M. Luteolin, a flavonoid with potential for cancer prevention and therapy. *Curr. Cancer Drug Tar.* **2008**, *8*(7), 634-646.
20. Cho, H., J.; Park, J., H., Y. Kaempferol induces cell cycle arrest in HT-29 human colon cancer cells. *J. Cancer prev*. **2013**, *18*(3), 257.
21. Weng, M., S.; Ho, Y., S.; Lin, J., K. Chrysin induces G1 phase cell cycle arrest in C6 glioma cells through inducing p21Waf1/Cip1 expression: involvement of p38 mitogen-activated protein kinase. *Biochem. Pharmacol.* **2005**, *69*(12), 1815-1827.
22. Choi, Y., H.; Lee, W., H.; Park, K., Y.; Zhang, L. p53-independent induction of p21 (WAF1/CIP1), reduction of cyclin B1 and G2/M arrest by the isoflavone genistein in human prostate carcinoma cells. *Jpn. J. Cancer Res.* **2000**, *91*(2), 164-173.
23. Grynberg, N., F.; Carvalho, M., D.; Velandia, J., R.; Oliveira, M., C.; Moreira, I., C.; Braz-Filho, R.; Echevarria, A. DNA topoisomerase inhibitors: biflavonoids from Ouratea species. *Braz. J. Med. Boil. Res.* **2002**, *35*(7), 819-822.
24. Kirby, G., C.; Paine, A.; Warhurst, D., C.; Noamese, B., K.; Phillipson, J., D. In vitro and in vivo antimalarial activity of cryptolepine, a plant-derived indoloquinoline. *Phytother. Res.* **1995**, *9*(5), 359-363.
25. Bonjean, K.; De-Pauw-Gillet, M., C.; Defresne, M., P.; Colson, P.; Houssier, C.; Dassonneville, L.; Bailly, C.; Greimers, R.; Wright, C.; Quetin-Leclercq, J.; Tits, M. The DNA intercalating alkaloid cryptolepine interferes with topoisomerase II and inhibits primarily DNA synthesis in B16 melanoma cells. *Biochemistry* **1998**, *37*(15), 5136-5146.
26. Bailly, C.; Laine, W.; Baldeyrou, B.; De, M., P., G.; Colson, P.; Houssier, C.; Cimanga, K.; Van, S., M.; Vlietinck, A., J.; Pieters, L. DNA intercalation, topoisomerase II inhibition and cytotoxic activity of the plant alkaloid neocryptolepine. *Anti-cancer Drug Des.* **2000**, *15*(3), 191-201.
27. Dassonneville, L.; Lansiaux, A.; Wattelet, A.; Wattez, N.; Mahieu, C.; Van-Miert, S.; Pieters, L.; Bailly, C. Cytotoxicity and cell cycle effects of the plant alkaloids cryptolepine and neocryptolepine: relation to drug-induced apoptosis. *Eur. J. Pharmacol.* **2000**, *409*(1),9-18.
28. Sun, N., J.; Woo, S., H.; Cassady, J., M; Snapka, R., M.; DNA polymerase and topoisomerase II inhibitors from Psoralea corylifolia. *J. Nat. Prod.* **1998**, *61*(3), 362-366.
29. Prescott, T., A.; Sadler, I., H.; Kiapranis, R.; Maciver, S., K. Lunacridine from Lunasia amara is a DNA intercalating topoisomerase II inhibitor. *J. Ethnopharmacol.* **2007**, *109*(2), 289-294.
30. Jo, J., Y.; Gonzalez-de-Mejia, E.; Lila, M., A. Catalytic inhibition of human DNA topoisomerase II by interactions of grape cell culture polyphenols. *J. Agr. Food Chem*. **2006**, *54*(6), 2083-2087.
31. Sugimoto, Y.; Tsukahara, S.; Oh-hara, T.; Liu, L., F.; Tsuruo, T. Elevated expression of DNA topoisomerase II in camptothecin-resistant human tumor cell lines. *Cancer Res*. **1990**, *50*(24), 7962-7965.
32. Lu, H., R.; Meng, L., H.; Huang, M.; Zhu, H.; Miao, Z., H.; Ding, J. DNA damage, c-myc suppression and apoptosis induced by the novel topoisomerase II inhibitor,

salvicine, in human breast cancer MCF-7 cells. *Cancer Chemoth. Pharm*. **2005**, *55*(3), 286-294.
33. Zhang, Y.; Wang, L.; Chen, Y.; Qing, C. Anti-angiogenic activity of salvicine. *Pharm. Boil*. **2013**, *51*(8), 1061-1065.
34. Lee, Y., K.; Seo, C., S.; Lee, C., S.; Lee, K., S.; Kang, S., J.; Jahng, Y.; Chang, H., W.; Son, J., K. Inhibition of DNA topoisomerases I and II and cytotoxicity by lignans from Saururus chinensis. *Arch. Pharm. Res*. **2009**, *32*(10), 1409.
35. Maas, J., L.; Galletta, G., J.; Stoner, G., D. Ellagic acid, an anticarcinogen in fruits, especially in strawberries: a review. *HortScience*. **1991**, *26*(1), 10-14.
36. Labrecque, L.; Lamy, S.; Chapus, A.; Mihoubi, S.; Durocher, Y.; Cass, B.; Bojanowski, M., W.; Gingras, D.; Béliveau, R. Combined inhibition of PDGF and VEGF receptors by ellagic acid, a dietary-derived phenolic compound. *Carcinogenesis*. **2005**, *26*(4), 821-826.
37. Tong, Q.; Qing, Y.; Wu, Y.; Hu, X.; Jiang, L.; Wu, X. Dioscin inhibits colon tumor growth and tumor angiogenesis through regulating VEGFR2 and AKT/MAPK signaling pathways. *Toxicol. Appl. Pharm*. **2014**, *281*(2), 166-173.
38. Cho, J.; Choi, H.; Lee, J.; Kim, M., S.; Sohn, H., Y.; Lee, D., G. The antifungal activity and membrane-disruptive action of dioscin extracted from Dioscorea nipponica. *Biomembrane* **2013**, *1828*(3), 1153-1158.
39. Xu, H., Y.; Pan, Y., M.; Chen, Z., W.; Lin, Y.; Wang, L., H.; Chen, Y., H.; Jie, T., T.; Lu, Y., Y. Liu, J., C. 12-Deoxyphorbol 13-palmitate inhibit VEGF-induced angiogenesis via suppression of VEGFR-2-signaling pathway. *J. Ethnopharmacol.* **2013**, *146*(3), 724-733.
40. Cerezo, A.; Hornedo-Ortega, R.; Álvarez-Fernández, M.; Troncoso, A.; García-Parrilla, M. Inhibition of VEGF-Induced VEGFR-2 activation and HUVEC migration by melatonin and other bioactive indolic compounds. *Nutrients* **2017**, *9*(3), 249.
41. Saraswati, S.; Kumar, S.; Alhaider, A., A. α-santalol inhibits the angiogenesis and growth of human prostate tumor growth by targeting vascular endothelial growth factor receptor 2-mediated AKT/mTOR/P70S6K signaling pathway. *Mol. Cancer* **2013**, *12*(1), 147.
42. Lai, L.; Liu, J.; Zhai, D.; Lin, Q.; He, L.; Dong, Y.; Zhang, J.; Lu, B.; Chen, Y.; Yi, Z.; Liu, M. Plumbagin inhibits tumour angiogenesis and tumour growth through the Ras signalling pathway following activation of the VEGF receptor-2. Brit. J. Pharmaco. **2012**, 165(4b), 1084-1096.
43. Jung, M., H.; Lee, S., H.; Ahn, E., M.; Lee, Y., M. Decursin and decursinol angelate inhibit VEGF-induced angiogenesis via suppression of the VEGFR-2-signaling pathway. *Carcinogenesis* **2009**, *30*(4), 655-661.
44. Jung, S., Y.; Choi, J., H.; Kwon, S., M.; Masuda, H.; Asahara, T.; Lee, Y., M. Decursin inhibits vasculogenesis in early tumor progression by suppression of endothelial progenitor cell differentiation and function. *J. Cell. Biochem.* **2012**, *113*(5), 1478-1487.
45. Lee, S.; Lee, Y., S.; Jung, S., H.; Shin, K., H.; Kim, B., K.; Kang, S., S. Anti-tumor activities of decursinol angelate and decursin fromAngelica gigas. *Arch. Pharm. Res*. **2003**, *26*(9), 727-730.

46. Pratheeshkumar, P.; Budhraja, A.; Son, Y., O.; Wang, X.; Zhang, Z.; Ding, S.; Wang, L.; Hitron, A.; Lee, J., C.; Xu, M.; Chen, G. Quercetin inhibits angiogenesis mediated human prostate tumor growth by targeting VEGFR-2 regulated AKT/mTOR/P70S6K signaling pathways. *PloS ONE* **2012**, *7*(10), e47516.
47. Miean, K., H.; Mohamed, S. Flavonoid (myricetin, quercetin, kaempferol, luteolin, and apigenin) content of edible tropical plants. *J. Agr. Food Chem.* **2001**, *49*(6), 3106-3112.
48. Nevins, J., R.; Leone, G.; DeGregori, J.; Jakoi, L. Role of the Rb/E2F pathway in cell growth control. *J. Cell. Physiol*. **1997**, *173*(2), 233-236.
49. De-Bondt, H., L.; Rosenblatt, J.; Jancarik, J.; Jones, H., D.; Morgant, D., O.; Kim, S., H. Crystal structure of cyclin-dependent kinase 2. *Nature* **1993**, *363*(6430), 595.
50. Sherr, C., J.; Roberts, J., M. CDK inhibitors: positive and negative regulators of G1-phase progression. *Gene. Dev.* **1999**, *13*(12), 1501-1512.
51. Ho, A.; Dowdy, S., F. Regulation of G1 cell-cycle progression by oncogenes and tumor suppressor genes. *Curr. Opin. Genet. Dev.* **2002**, *12*(1), 47-52.
52. Shapiro, G., I. Cyclin-dependent kinase pathways as targets for cancer treatment. *J. Clin. Oncol*. **2006**, *24*(11), 1770-1783.
53. Boonstra, J. Progression through the G1-phase of the on-going cell cycle. *J. Cell. Biochem.* **2003**, *90*(2), 244-252.
54. Harper, J., W.; Elledge, S., J. Cdk inhibitors in development and cancer. *Curr. Opin. Genet. Dev.* **1996**, 6(1), 56-64.
55. Ullah, A.; Prottoy, N., I.; Araf, Y.; Hossain, S.; Sarkar, B.; Saha, A. Molecular Docking and Pharmacological Property Analysis of Phytochemicals from Clitoria ternatea as Potent Inhibitors of Cell Cycle Checkpoint Proteins in the Cyclin/CDK Pathway in Cancer Cells. *Comput. Mol. Biosci.* **2019**, *9*(03), 81.
56. Benson, C.; Kaye, S.; Workman, P.; Garrett, M.; Walton, M.; De-Bono, J. Clinical anticancer drug development: targeting the cyclin-dependent kinases. *Br. J. Cancer* **2005**, *92*(1), 7.
57. Deweese, J., E.; Osheroff, N. The DNA cleavage reaction of topoisomerase II: wolf in sheep's clothing. *Nucleic Acids Res.* **2008**, *37*(3), 738-748.
58. Nitiss, J., L. Targeting DNA topoisomerase II in cancer chemotherapy. *Nat. Rev. Cancer* **2009**, *9*(5), 338.
59. Russo, P.; Del-Bufalo, A.; Cesario, A. Flavonoids acting on DNA topoisomerases: recent advances and future perspectives in cancer therapy. *Curr. Med. Chem.* **2012**, *19*(31), 5287-5293.
60. Ashour, M., E.; Atteya, R.; El-Khamisy, S., F. Topoisomerase-mediated chromosomal break repair: an emerging player in many games. *Nat. Rev. Cancer* **2015**, *15*(3), 137-151.
61. Christmann-Franck, S.; Bertrand, H., O.; Goupil-Lamy, A.; Der-Garabedian, P., A.; Mauffret, O.; Hoffmann, R.; Fermandjian, S. Structure-based virtual screening: an application to human topoisomerase II α. *J. Med. Chem.* **2004**, *47*(27), 6840-6853.
62. Folkman, J. 1984. Angiogenesis. In *Biology of endothelial cells* (pp. 412-428). Springer, Boston, MA.

63. Ferrara, N.; Davis-Smyth, T. The biology of vascular endothelial growth factor. *Endocr. Rev.* **1997**, *18*(1),.4-25.
64. Nowak, D., G.; Woolard, J.; Amin, E., M.; Konopatskaya, O.; Saleem, M., A.; Churchill, A., J.; Ladomery, M., R.; Harper, S., J.; Bates, D., O. Expression of pro-and anti-angiogenic isoforms of VEGF is differentially regulated by splicing and growth factors. *J. Cell Sci.* **2008**, *121*(20), 3487-3495.
65. Kim, K., J.; Li, B.; Winer, J.; Armanini, M.; Gillett, N.; Phillips, H., S.; Ferrara, N. Inhibition of vascular endothelial growth factor-induced angiogenesis suppresses tumour growth in vivo. *Nature* **1993**, *362*(6423), 841.
66. Ma, X.; Ma, C., X.; Wang, J. Endometrial carcinogenesis and molecular signaling pathways. *Am. J. Mol. Biol.* **2014**, 4(03), 134.
67. Rini, B., I.; Vascular endothelial growth factor–targeted therapy in renal cell carcinoma: current status and future directions. *Clin. Cancer Res.* **2007**, *13*(4), 1098-1106.
68. Melincovici, C., S.; Bosca, A., B.; Susman, S.; Marginean, M.; Mihu, C.; Istrate, M.; Moldovan, I., M.; Roman, A., L.; Mihu, C., M. Vascular endothelial growth factor (VEGF)-key factor in normal and pathological angiogenesis. *Rom. J. Morphol. Embryol*. **2018**, *59*(2), 455-467.
69. Roskoski-Jr, R.; Vascular endothelial growth factor (VEGF) and VEGF receptor inhibitors in the treatment of renal cell carcinomas. *Pharmacol. Res.* **2017,** 120, 116-132.
70. Schrödinger Release 2018-4: Maestro (2018), Schrödinger, LLC, New York, NY.
71. Visualizer, D.S. (2017) Release 4.1. Accelrys Inc., San Diego, CA.
72. Schrödinger Release 2018-4: Protein Preparation Wizard; Epik, Schrödinger, LLC, New York, NY, 2016; Impact, Schrödinger, LLC, New York, NY, 2016; Prime, Schrödinger, LLC, New York, NY, 2018.
73. Schrödinger Release 2018-4: Prime, Schrödinger, LLC, New York, NY, 2018.
74. Schrödinger Release 2018-4: LigPrep, Schrödinger, LLC, New York, NY, 2018.
75. Schrödinger Release 2018-4: Epik, Schrödinger, LLC, New York, NY, 2018.
76. Schrödinger Release 2018-4: Glide, Schrödinger, LLC, New York, NY, 2018.
77. Lipinski, C., A.; Lombardo, F.; Dominy, B., W.; Feeney, P., J. Experimental and computational approaches to estimate solubility and permeability in drug discovery and development settings. *Adv. Drug Deliv. Rev.* **1997**, *23*(1-3), 3-25.
78. Cheng, F.; Li, W.; Zhou, Y.; Shen, J.; Wu, Z.; Liu, G.; Lee, P., W.; Tang, Y. 2012. admetSAR: a comprehensive source and free tool for assessment of chemical ADMET properties.
79. Dong, J.; Wang, N., N.; Yao, Z., J.; Zhang, L.; Cheng, Y.; Ouyang, D.; Lu, A., P.; Cao, D., S. ADMETlab: a platform for systematic ADMET evaluation based on a comprehensively collected ADMET database. *J. Cheminformatics* **2018**, *10*(1), 29.
80. Filimonov, D., A.; Lagunin, A., A.; Gloriozova, T., A.; Rudik, A., V.; Druzhilovskii, D., S.; Pogodin, P., V.; Poroikov, V., V. Prediction of the biological activity spectra of organic compounds using the PASS online web resource. *Chem. Heterocycl. Compd*. **2014**, *50*(3), 444-457.

81. Geronikaki, A.; Poroikov, V.; Hadjipavlou-Litina, D.; Filimonov, D.; Lagunin, A.; Mgonzo, R. Computer aided predicting the biological activity spectra and experimental testing of new thiazole derivatives. *Quant. Struct.-act. Rel.* **1999**, *18*(1), 16-25.
82. Zaretzki, J.; Bergeron, C.; Huang, T., W.; Rydberg, P.; Swamidass, S., J.; Breneman, C., M. RS-WebPredictor: a server for predicting CYP-mediated sites of metabolism on drug-like molecules. *Bioinformatics* **2012**, *29*(4), 497-498.
83. Drwal, M., N.; Banerjee, P.; Dunkel, M.; Wettig, M., R.; Preissner, R. ProTox: a web server for the in silico prediction of rodent oral toxicity. *Nucleic Acids Res.* **2014**, *42*(W1), W53-W58.
84. Schrödinger Release 2018-4**:** Phase, Schrödinger, LLC, New York, NY, 2018.
85. Schrödinger Release 2018-4: QikProp, Schrödinger, LLC, New York, NY, 2018.
86. Schrödinger Release 2018-4: Jaguar, Schrödinger, LLC, New York, NY, 2018.

87. Lee, C.; Yang, W.; Parr, R., G. Development of the Colle-Salvetti correlation-energy formula into a functional of the electron density. *Phys. Rev. B* **1988**, *37*(2), 785.
88. Becke, A., D. Density-functional exchange-energy approximation with correct asymptotic behavior. *Phys. Rev. A* **1988**, *38*(6), 3098.
89. Pearson, R., G. Absolute electronegativity and hardness correlated with molecular orbital theory. *P. Natl. Acad. Sci.* **1986**, *83*(22), 8440-8441.
90. Parr, R., G.; Yang, W. Density-Functional Theory of Atoms and Molecules, vol. 16 of International series of monographs on chemistry. *Oxford University Press* **1989**, New York.

91. Awan, F.; Obaid, A.; Ikram, A; Janjua, H. Mutation-structure-function relationship based integrated strategy reveals the potential impact of deleterious missense mutations in autophagy related proteins on hepatocellular carcinoma (HCC): A comprehensive informatics approach. *Int. J. Mol. Sci.* **2017**, *18*(1), 139.

92. Prabhakar, P.-K.; Srivastava, A.; Rao, K.-K.; Balaji, P.-V. Monomerization alters the dynamics of the lid region in Campylobacter jejuni CstII: an MD simulation study. *J. Biomol. Struct. Dyn.* **2016**, *34*(4), 778-791. doi: 10.1080/07391102.2015.1054430

93. López-Blanco, J.-R.; Aliaga, J.-I.; Quintana-Ortí, E.-S.; Chacón, P. iMODS: internal coordinates normal mode analysis server. *Nucleic Acids Res.*, **2014**, *42*(W1), W271-W276.

94. Lopéz-Blanco, J.-R.; Garzón, J.-I.; Chacón, P. iMod: multipurpose normal mode analysis in internal coordinates. *Bioinformatics*, *27*(20), **2011**, 2843-2850.

95. Kovacs, J.-A.; Chacón, P.; Abagyan, R. Predictions of protein flexibility: first-order measures. *Proteins: Struct., Funct., Bioinf.*, **2004**, *56*(4), 661-668.

96. file:///C:/Program%20Files/Schrodinger20184/docs/Documentation.htm#maestro_tools_help/ramachandran_panel.html

97. Yuriev, E.; Ramsland, P., A. Latest developments in molecular docking: 2010–2011 in review. *J. Mol. Recognit.* **2013**, *26*(5), 215-239.
98. Prottoy, N.I., Sarkar, B., Ullah, A., Hossain, S., Boby, A.S. and Araf, Y., 2019. Molecular Docking and Pharmacological Property Analysis of Antidiabetic Agents from Medicinal Plants of Bangladesh against Type II Diabetes: A Computational Approach. *PharmaTutor*, *7*(9), pp.6-15.
99. Sarkar, B., Islam, S.S., Ullah, M.A., Hossain, S., Prottoy, M.N.I., Araf, Y. and Taniya, M.A., 2019. Computational Assessment and Pharmacological Property Breakdown of Eight Patented and Candidate Drugs against Four Intended Targets in Alzheimer's Disease. *Advances in Bioscience and Biotechnology*, *10*(11), p.405.
100. Zhang, X.; Perez-Sanchez, H.; C-Lightstone, F. A comprehensive docking and MM/GBSA rescoring study of ligand recognition upon binding antithrombin. *Curr. Top. Med. Chem.* **2017**, *17*(14), 1631-1639.
101. Sherman, W.; Day, T.; Jacobson, M., P.; Friesner, R., A.; Farid, R. Novel procedure for modeling ligand/receptor induced fit effects. *J. Med. Chem.* **2006**, *49*(2), 534-553.
102. Aamir, M.; Singh, V., K.; Dubey, M., K.; Meena, M.; Kashyap, S., P.; Katari, S., K.; Upadhyay, R., S.; Singh, S. In silico Prediction, Characterization, Molecular Docking and Dynamic Studies on Fungal SDRs as Novel Targets for Searching Potential Fungicides against Fusarium Wilt in Tomato. *Front. Pharmacol.* **2018**, *9*, 1038.
103. Friesner, R., A.; Murphy, R., B.; Repasky, M., P.; Frye, L., L.; Greenwood, J., R.; Halgren, T., A.; Sanschagrin, P., C.; Mainz, D., T. Extra precision glide: Docking and scoring incorporating a model of hydrophobic enclosure for protein− ligand complexes. *J. Med. Chem.* **2006**, *49*(21), 6177-6196.
104. Priyadarshini, V.; Pradhan, D.; Munikumar, M.; Swargam, S.; Umamaheswari, A.; Rajasekhar, D. Genome-based approaches to develop epitope-driven subunit vaccines against pathogens of infective endocarditis. *J. Biomol. Struct. Dyn.* **2014**, *32*(6), 876-889.
105. Lipinski, C., A.; Lead-and drug-like compounds: the rule-of-five revolution. *Drug Discov. Today Technol.* **2004**, *1*(4), 337-341.
106. Sander, T. OSIRIS property explorer. *Organic Chemistry Portal*. **2001**
107. Pollastri, M., P. Overview on the Rule of Five. *Curr. Protoc. Pharmacol*. **2010**, *49*(1), 9-12.
108. Ghose, A., K.; Viswanadhan, V., N.; Wendoloski, J., J. A knowledge-based approach in designing combinatorial or medicinal chemistry libraries for drug discovery. 1. A qualitative and quantitative characterization of known drug databases. *J. Comb. Chem.* **1999**, *1*(1), 55-68.
109. Veber, D., F.; Johnson, S., R.; Cheng, H., Y.; Smith, B., R.; Ward, K., W.; Kopple, K., D. Molecular properties that influence the oral bioavailability of drug candidates. *J. Med. Chem.* **2002**, *45*(12), 2615-2623.
110. Egan, W., J.; Merz, K., M.; Baldwin, J., J. Prediction of drug absorption using multivariate statistics. *J. Med. Chem.* **2000**, *43*(21), 3867-3877.
111. Muegge, I.; Heald, S., L.; Brittelli, D. Simple selection criteria for drug-like chemical matter. *J. Med. Chem.* **2001**, *44*(12), 1841-1846.

112. Ertl, P.; Schuffenhauer, A. Estimation of synthetic accessibility score of drug-like molecules based on molecular complexity and fragment contributions. *J. Cheminformatics* **2009**, *1*(1), 8.
113. Martin, Y., C. A bioavailability score. *J. Med. Chem.* **2005**, *48*(9), 3164-3170.
114. Li, A., P. Screening for human ADME/Tox drug properties in drug discovery. *Drug Discov. Today* **2001**, *6*(7), 357-366.
115. Guengerich, F., P. Cytochrome P-450 3A4: regulation and role in drug metabolism. *Annu. Rev. Pharmacol. Toxicol.* **1999**, *39*(1), 1-17.
116. Glue, P.; Clement, R., P. Cytochrome P450 enzymes and drug metabolism—basic concepts and methods of assessment. *Cell. Mol. Neurobiol.* **1999**, *19*(3), 309-323.
117. Dixit, B. A review on the effects of CMPF binding with Human Serum Albumin. *Bioinformatics Rev.* **2017**, *3*(9), 9-18.
118. Radchenko, E., V.; Dyabina, A., S.; Palyulin, V., A.; Zefirov, N., S. Prediction of human intestinal absorption of drug compounds. *Russ. Chem. Bull.* **2016**, *65*(2), 576-580.
119. Wessel, M., D.; Jurs, P., C.; Tolan, J., W.; Muskal, S., M. Prediction of human intestinal absorption of drug compounds from molecular structure. *J. Chem. Inf. Comput. Sci*. **1998**, *38*(4), 726-735.
120. Basant, N.; Gupta, S.; Singh, K., P. Predicting human intestinal absorption of diverse chemicals using ensemble learning based QSAR modeling approaches. *Comput. Biol. Chem.* **2016**, *61*, 178-196.
121. Swierczewska, M.; Lee, K., C.; Lee, S. What is the future of PEGylated therapies?. **2015**
122. Smalling, R., W. Molecular biology of plasminogen activators: what are the clinical implications of drug design?. *Am. J. Cardiol.* **1996**, *78*(12), 2-7.
123. Sahin, S.; Benet, L., Z. The operational multiple dosing half-life: a key to defining drug accumulation in patients and to designing extended release dosage forms. *Pharm. Res.* **2008**, *25*(12), 2869-2877.
124. Sanguinetti, M., C.; Jiang, C.; Curran, M., E.; Keating, M., T. A mechanistic link between an inherited and an acquird cardiac arrthytmia: HERG encodes the IKr potassium channel. *Cell* **1995**, *81*(2), 299-307.
125. Aronov, A., M. Predictive in silico modeling for hERG channel blockers. *Drug Discov. Today* **2005**, *10*(2), 149-155.
126. Cheng, A.; Dixon, S., L. In silico models for the prediction of dose-dependent human hepatotoxicity. *J. Comput. Aid. Mol. Des.* **2003**, *17*(12), 811-823.
127. Xu, J., J.; Diaz, D.; O'Brien, P., J. Applications of cytotoxicity assays and pre-lethal mechanistic assays for assessment of human hepatotoxicity potential. *Chem. Biol. Interact.* **2004**, *150*(1), 115-128.
128. Mortelmans, K.; Zeiger, E. The Ames Salmonella/microsome mutagenicity assay. *Mutat. Res-Fund Mol. M*. **2000**, *455*(1-2), 29-60.
129. Holt, M., P.; Ju, C. Mechanisms of drug-induced liver injury. *AAPS J.* **2006**, *8*(1), E48-E54.

130. Lagunin, A.; Stepanchikova, A.; Filimonov, D.; Poroikov, V. PASS: prediction of activity spectra for biologically active substances. *Bioinformatics* **2000**, *16*(8), 747-748.
131. United Nations. Economic Commission for Europe. Secretariat, 2005. *Globally harmonized system of classification and labelling of chemicals (GHS)*. United Nations Publications.
132. Tyzack, J., D.; Mussa, H., Y.; Williamson, M., J.; Kirchmair, J.; Glen, R., C. Cytochrome P450 site of metabolism prediction from 2D topological fingerprints using GPU accelerated probabilistic classifiers. *J. Cheminformatics* **2014**, *6*(1), 29.
133. Danielson, P., B. The cytochrome P450 superfamily: biochemistry, evolution and drug metabolism in humans. *Curr. Drug Metab.* **2002**, *3*(6), 561-597.
134. Dixon, S., L.; Smondyrev, A., M.; Knoll, E., H.; Rao, S., N.; Shaw, D., E.; Friesner, R., A. PHASE: a new engine for pharmacophore perception, 3D QSAR model development, and 3D database screening: 1. Methodology and preliminary results. *J. Comput. Aid. Mol. Des.* **2006**, *20*(10-11), 647-671.
135. Hussain, A.; Verma, C., K. A Combination of Pharmacophore Modeling, Molecular Docking and Virtual Screening Study Reveals 3, 5, 7-Trihydroxy-2-(3, 4, 5-trihydroxyphenyl)-4H-Chromen-4-One as a Potential Anti-Cancer Agent of COT Kinase. *Indian J. Pharm. Educ. Res.* **2018**, *52*(4), 699-706.
136. Matysiak, J. Evaluation of electronic, lipophilic and membrane affinity effects on antiproliferative activity of 5-substituted-2-(2, 4-dihydroxyphenyl)-1, 3, 4-thiadiazoles against various human cancer cells. *Eur. J. Med. Chem.* **2007**, *42*(7), 940-947.
137. Zhan, C., G.; Nichols, J., A.; Dixon, D., A. Ionization potential, electron affinity, electronegativity, hardness, and electron excitation energy: molecular properties from density functional theory orbital energies. *J. Phys. Chem. A* **2003**, *107*(20), 4184-4195.
138. Hoque, M., M.; Halim, M., A.; Sarwar, M., G.; Khan, M., W. Palladium-catalyzed cyclization of 2-alkynyl-N-ethanoyl anilines to indoles: synthesis, structural, spectroscopic, and mechanistic study. *J. Phys. Org. Chem.* **2015**, *28*(12), 732-742.
139. Ayers, P., W.; Parr, R., G.; Pearson, R., G. Elucidating the hard/soft acid/base principle: a perspective based on half-reactions. *J. Chem. Phys.* **2006**, *124*(19), 194107.

140. Hung, P.-F.; Wu, B.-T.; Chen, H.-C.; Chen, Y.-H.; Chen, C.-L.; Wu, M.-H.; Liu, H.-C.; Lee, M.-J.; Kao, Y.-H. Antimitogenic effect of green tea (−)-epigallocatechin gallate on 3T3-L1 preadipocytes depends on the ERK and Cdk2 pathways. *Am. J. Physiol-Cell*. *288*(5), **2005**, C1094-C1108.

141. Snyder, R.-D.; Gillies, P.-J. Evaluation of the clastogenic, DNA intercalative, and topoisomerase II-interactive properties of bioflavonoids in Chinese hamster V79 cells. *Environ. Mol. Mutagen.* **2002**, *40*(4), 266-276.

142. Balakrishnan, S.; Bhat, F.-A.; Raja Singh, P.; Mukherjee, S.; Elumalai, P.; Das, S.; Patra, C.-R.; Arunakaran, J. Gold nanoparticle–conjugated quercetin inhibits epithelial–mesenchymal transition, angiogenesis and invasiveness via EGFR/VEGFR-2-mediated pathway in breast cancer. *Cell prolif.* **2016**, *49*(6), 678-697.

143. Donnini, S.; Finetti, F.; Lusini, L.; Morbidelli, L.; Cheynier, V.; Barron, D.; Williamson, G.; Waltenberger, J.; Ziche, M. Divergent effects of quercetin conjugates on angiogenesis. *Br. J. Nutr.* **2006**, *95*(5), 1016-1023.

144. Namita, P.; Mukesh, R.; Vijay, K., J. Camellia sinensis (green tea): A review. *Global J. Pharm.* **2012**, *6*(2), 52-59.

145. Bouque, V.; Bourgaud, F.; Nguyen, C.; Guckert, A. Production of daidzein by callus cultures of Psoralea species and comparison with plants. *Plant Cell Tiss. Org.* **1998**, *53*(1), 35-40.

146. Yu, O.; Jung, W.; Shi, J.; Croes, R., A.; Fader, G., M.; McGonigle, B.; Odell, J., T. Production of the isoflavones genistein and daidzein in non-legume dicot and monocot tissues. *Plant Physiol.* **2000**, *124*(2), 781-794.

147. Yu, O.; Jung, W.; Shi, J.; Croes, R., A.; Fader, G., M.; McGonigle, B.; Odell, J., T. Production of the isoflavones genistein and daidzein in non-legume dicot and monocot tissues. *Plant Physiol.* **2000**, *124*(2), 781-794.